1965

Investigations of yttrium-iron-garnet materials in coaxial coupling structures for preselector applications

William Stevens Elliott
Iowa State University

INVESTIGATIONS OF YTTRIUM-IRON-GARNET MATERIALS IN COAXIAL COUPLING STRUCTURES FOR PRESELECTOR APPLICATIONS

by

William Stevens Elliott

A Dissertation Submitted to the
Graduate Faculty in Partial Fulfillment of
The Requirements for the Degree of
DOCTOR OF PHILOSOPHY

Major Subject: Electrical Engineering

Approved:

Signature was redacted for privacy.

In Charge of Major Work

Signature was redacted for privacy.

Head of Major Department

Signature was redacted for privacy.

Dean of Graduate College

Iowa State University
Of Science and Technology
Ames, Iowa

1965

TABLE OF CONTENTS

I. INTRODUCTION

A. Purpose of Investigation

The purpose of this investigation was to study in analytical and experimental detail the application of low-loss, single-crystal yttrium-iron-garnet (YIG) materials operating at ferrimagnetic resonance in coaxial coupling structures. Since an inductively coupled magnetic resonator biased with a dc magnetic field is equivalent to a high-Q inductively coupled lumped parameter resonant circuit, both band pass and band reject filters can be constructed using these ferrite resonators. The main application of these filters would be for use as tunable pre-selectors in uhf and microwave receivers. Power limiters, circulators, isolators and other microwave devices using the magnetic properties of YIG can also be constructed but such applications were beyond the scope of this investigation.

In previous band pass applications the transmission structures (coaxial, stripline or waveguide) have been constructed so that the YIG resonator was located at a point of high magnetic field intensity. The input and output lines were electromagnetically coupled to the YIG resonator but were not coupled to each other in the absence of the resonator. In most band reject applications the YIG resonator produced a discontinuity at ferrimagnetic resonance.

The purpose of this study was to investigate a coaxial coupling structure containing an iris which permitted electromagnetic coupling between input and output transmission lines. As a result of both aperture and YIG resonator coupling, a "discriminator" transmission characteristic

was obtained. At the two extremes of aperture coupling, represented by either a very small iris aperture or a uniform line without an iris, the device behaves as either a band pass or band reject filter, respectively.

B. Applications

In many of the most modern systems concepts in the microwave field it is desirable to use narrow-band filters capable of rapid tuning or sweeping over frequency ranges of an octave or greater. Narrow-band filters consisting of quarter- or half-wavelength coaxial lines, cavities, etc., are seriously limited in these applications by the accuracy and speed of mechanical tuning. Ferrimagnetic resonators are of interest because they can be used in the construction of electronically tunable filters whose pass (reject) band center frequencies can be varied by changing the strength of a biasing dc magnetic field. The unloaded Q of these resonators compares favorably with the Q's of transmission-line and hollow cavity resonators.

In a qualitative sense, the basic principle of operation of a band pass ferrimagnetic resonator filter with maximum attenuation away from resonance is illustrated in Figure 1. A small ferrite ellipsoid (typically a sphere 0.015 to 0.1 inch in diameter) is placed at the intersection of two coils which are physically placed along the x- and y-axes so that there is no mutual coupling between them. Without a dc magnetic bias field there is no interaction between the coils and the ferrite ellipsoid. However, when a dc magnetic field is applied along the z-axis, the ferrite becomes magnetized with its magnetic moment vector aligned parallel with the dc magnetic field. Then an rf driving current in one

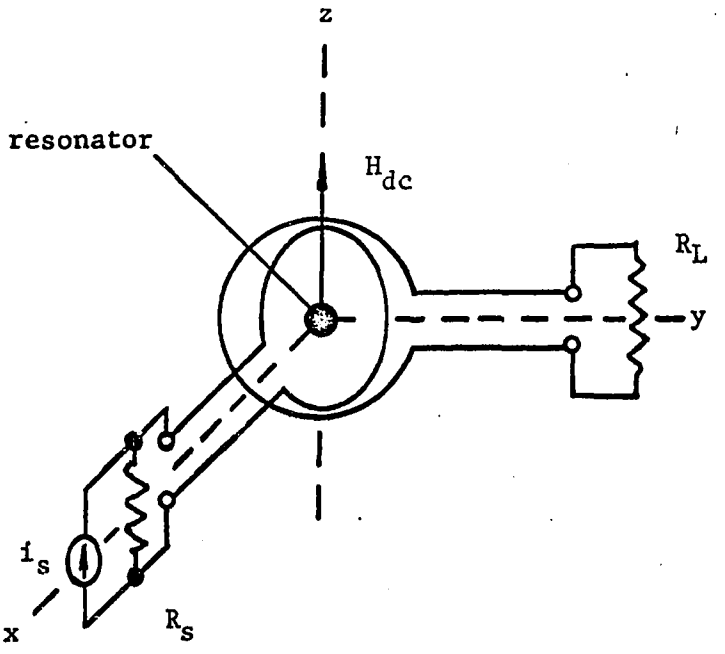

Figure 1. Coupling principle for a ferrimagnetic resonator filter

coil, say the x-axis coil, couples with the magnetic moment of the ferrite ellipsoid and causes the magnetic moment vector to precess about the z-axis. The precession of the magnetic moment couples with the y-axis coil and induces a voltage. The induced voltage is largest when the signal frequency is at the ferrimagnetic resonance frequency of the ferrite. This frequency is a function of the intensity of the dc magnetic field and the detailed shape of the ellipsoid. The magnitude of the coupled response away from resonance is determined by the degree of coupling between the coils and the magnetic moment of the ferrite ellipsoid and by the internal losses of the ferrite. Since the ferrimagnetic resonance frequency depends primarily upon the dc magnetic field intensity, tuning can be accomplished by varying the applied field; the frequency range is limited mainly by the bandwidth of the coupling configuration.

Ferrite materials have been used in microwave devices since the mid-1950's (1, 2, 3), but early materials were polycrystalline in nature and also electromagnetic coupling between the ferrite and microwave fields was very loose. Consequently the effect of the ferrite was usually satisfactorily treated as a perturbation of the normal field problem. The use of single-crystal YIG spheres and tight coupling was first reported in 1959 by De Grasse (4) who used tuned stripline coupling structures. The structure, shown in Figure 2, contained crossed stripline input and output transmission lines terminated in short circuits. The intersection of the lines was located at a distance from the shorted ends corresponding to one-half wavelength at the center of the tuning range. The YIG sphere, located at the intersection, was therefore at a point of high magnetic

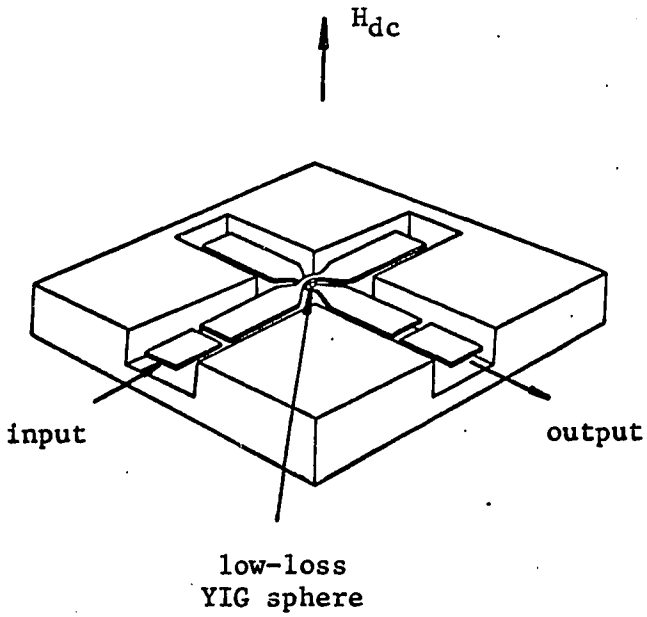

Figure 2. Stripline coupling structure used by DeGrasse (4)

field. To obtain coupling between the magnetic moment of the YIG and the microwave fields of the two transmission lines, the dc magnetic bias field was aligned vertically.

A practical problem associated with this structure is of interest. Since the physical lengths of transmission line between the intersection and the shorted ends are fixed, the resonator will not remain at a point of nearly maximum magnetic field as frequency is varied. This variation in coupling will limit the practical tuning range. Nevertheless, this technique for concentrating the microwave magnetic field is used widely in magnetically tunable coupling structures.

Since 1959 a number of investigators have reported their work, including Carter (5, 6), Patel (7), Kotzebue (8) and others (9, 10). The coupling principle for a single-resonator waveguide filter investigated by Carter at 8 to 11 gigacycles per second (gc/s) is shown in Figure 3. In this case the cross-sections of the two waveguides have been rotated ninety degrees so that transverse electromagnetic fields in the input guide will be unable to propagate in the output waveguide. The dc magnetic bias field is applied along the common axis of the waveguides by using E-plane circular bends and a "C"-type electromagnet. The coupling arrangement is analogous to the crossed loops since the YIG sphere is mounted in a styrofoam support in the open region common to the input and output waveguides. The depth of penetration as well as resonator and guide sizes can be varied to control coupling. In this structure the position of the resonator remains at a point of nearly maximum magnetic field as frequency is varied, therefore this form of coupling is preferable where a broad tuning range is desired.

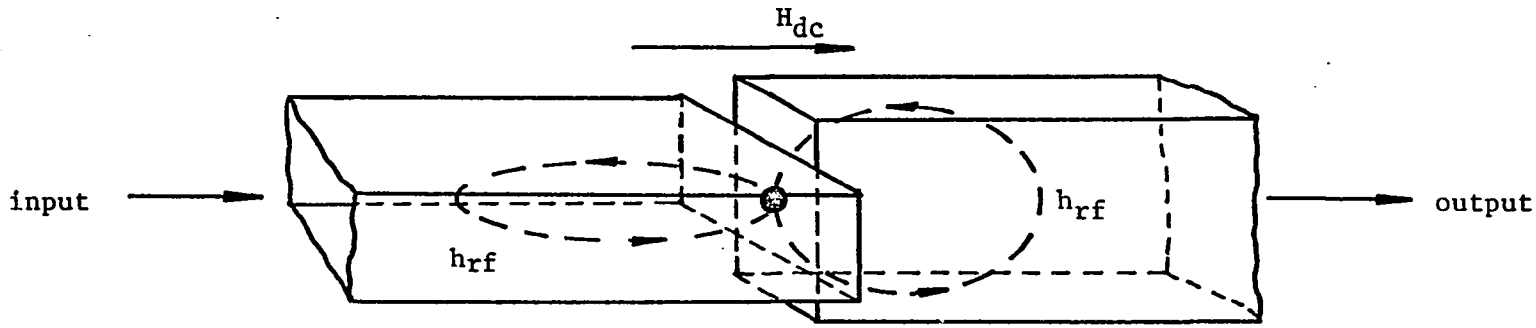

Figure 3. Coupling principle for waveguide ferrimagnetic resonator filter

Carter (6) has also described a two-resonator filter tunable between 8 and 14 gc/s as shown in Figure 4. Coupling between the resonators is accomplished by a long-slot iris in a 0.010-inch thick conducting wall which separates the input and output waveguides. The long vertical coupling slot permits the vertical components of rf magnetic moment to be coupled through their external fields, but prevents the horizontal magnetic fields of the waveguide and the horizontal magnetic moments from being coupled.

Standard band pass devices tunable over a frequency octave are being built commercially in frequency ranges from one to 18 gc/s with instantaneous bandwidths from 10 to 50 megacycles per second (mc/s) and insertion losses of approximately one decibel (db) per stage. Research and development is continuing to extend the frequency range to both higher and lower frequencies and to increase the range of control to several octaves.

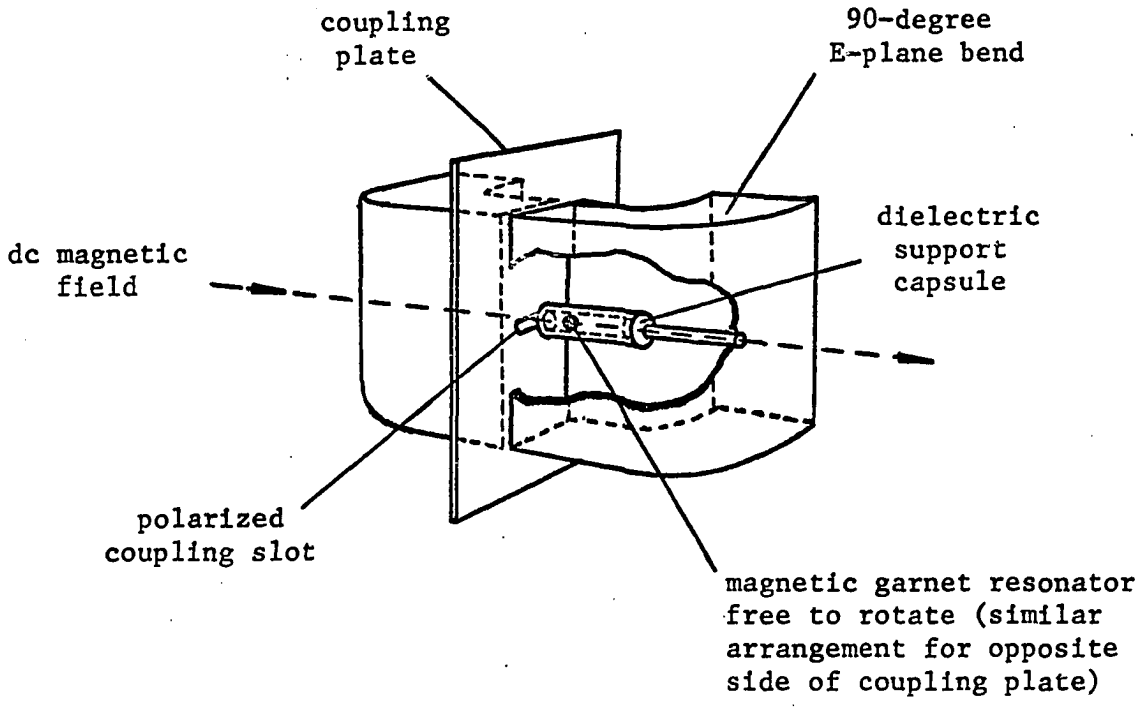

Figure 4. Two-resonator 8 to 14 gc/s filter described by Carter (6)

II. PROPERTIES OF FERRIMAGNETIC RESONATOR MATERIALS

According to Harrison and Hodges (11), approximately one-half of the metal ions in the periodic table have been put in the crystal structure of garnets, but only a few of these are ferrimagnetic above room temperature. The following single-crystal materials have possible use as ferrimagnetic resonators and are of interest at this time (12 thru 15):

(a) Yttrium-iron-garnet (YIG),

(b) Gallium-substituted yttrium-iron-garnet (Ga-YIG),

(c) Lithium ferrite and

(d) Barium ferrite.

The YIG material has been most useful to date. Since the detailed theory of ferrimagnetic resonance can be found in Lax and Button (16), Dekker (17) or various other references, only a qualitative description of ferrimagnetic resonance and some basic formulas and concepts useful in the design of magnetically tunable filters will be presented here.

A. Qualitative Description of Ferrimagnetic Resonance

In the "quasi-classical" theory, the magnetic moment of the electron arises from its spinning motion, thus the electron can be regarded as a spinning magnetic top. If an electron is placed in a static magnetic field that is not parallel to its magnetic moment vector, the torque exerted on the electron by the magnetic field causes the electron to precess about the axis of the field at the Larmor angular frequency

$$\omega_o = \mu_o \gamma H_{dc} \tag{1}$$

where μ_o is the permeability of free space, γ is the gyromagnetic

ratio of the electron spin and H_{dc} is the applied dc magnetic field intensity. For a magnetic field intensity expressed in oersteds[1], the frequency in mc/s is

$$(f_o)_{mc} = 2.8\ H_{dc}. \qquad (2)$$

The magnetic moment of the electron is represented in Figure 5(A) by the vector M_e precessing about the applied dc magnetic field. This rotating magnetic moment produces a circularly polarized magnetic field in a plane perpendicular to the applied field. If a circularly polarized microwave H-field is applied as indicated by the rotating h+ vector in Figure 5(B), the electron spin absorbs energy from the field. The nearer the frequency of the microwave field is to the natural precession frequency, the greater will be the energy absorbed by the spin. However, if a circularly polarized field is applied with polarization in the opposite direction as indicated by the rotating h- vector in Figure 5(C), the electron will not absorb energy from the applied field even if the signal is at the natural precession frequency. Thus, the absorption of energy, or resonance phenomenon, is non-reciprocal.

When a macroscopic sample of a ferrimagnetic material is placed in a dc magnetic field and subjected to a microwave magnetic field it will display a similar gyromagnetic resonance phenomenon. However, the frequency of resonance will differ from that of a free electron due to mutual interactions between the electron spins within the material and a

---

[1]The most commonly used unit for magnetic field intensity has been the oersted. The value can be converted to MKS units by use of the conversion H_{dc} (in ampere-turns/meter) = 79.5 H_{dc} (in oersteds).

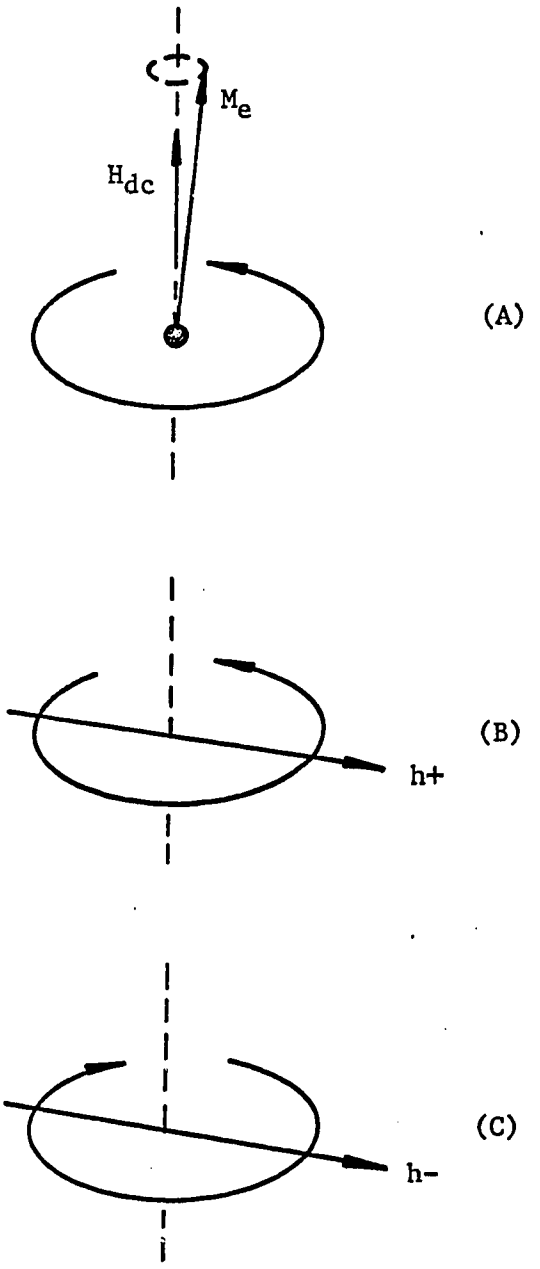

Figure 5. (A) Circularly polarized magnetic field of a precessing electron

(B) and (C) External circularly polarized rf magnetic fields

difference between the fields inside the material and those applied externally. The field differences are caused by shape demagnetizing effects, magnetic anisotropy, crystalline imperfections, etc.

The resonance conditions and microwave susceptibility of a macroscopic sample of the material can be obtained by starting with the equation of motion of the magnetic moment. The modified Landau-Lifshitz representation may be written in MKS units as

$$\vec{dM}/dt = \gamma\ (\vec{M} \times \vec{H}) - (\alpha/|M|)\ (\vec{M} \times \vec{dM}/dt), \tag{3}$$

where $\vec{M}$ is the magnetic moment per unit volume, γ is the gyromagnetic ratio of the electron spin (as before), α is the phenomenological damping constant and $\vec{H}$ is the vector sum of all the magnetic fields seen by the spinning electrons. The damping term is most accurate when the dc field is sufficient to saturate the material and will be discussed briefly later.

To evaluate the magnetic field inside a finite ferrimagnetic sample in the presence of an electromagnetic field, it is necessary in principle to solve the associated boundary-valve problem. This task is complicated and often impossible in practice. However, if the ferrite samples are small compared with a wavelength, the field inside the sample has uniform intensity although it differs from the external field because of the discontinuity of the normal component of the susceptibility at the boundary. For arbitrary shapes the problem is still difficult to solve, but solutions have been obtained for small ellipsoidal samples in a uniform external field (18). The internal field is then given by

$$\vec{H} = \vec{H}_{ext} - \overleftrightarrow{N} \cdot \vec{M}, \tag{4}$$

where $\overleftrightarrow{N} \cdot \vec{M}$ is an opposing internal field due to the presence of magnetic dipoles induced on the surface by the applied field. The demagnetizing tensor $\overleftrightarrow{N}$ is a measure of this induction and depends on the ratio of the ellipsoidal dimensions. The components of $\overleftrightarrow{N}$ satisfy the relation $N_x + N_y + N_z = 1$. (NOTE: Additional terms can be introduced in Equation 4 to account for the demagnetizing effects caused by magnetic anisotropy, but they will be neglected here.)

In general, both the magnetic moment and magnetic field vectors contain static and alternating components which may be written as

$$\vec{M} = \vec{M}_s + \vec{m}\epsilon^{j\omega t} \tag{5}$$

and

$$\vec{H}_{ext} = \vec{H}_{dc} + \vec{h}\epsilon^{j\omega t}, \tag{6}$$

where $\vec{M}_s$ is the saturation magnetization vector per unit volume and $\vec{m}$ and $\vec{h}$ are rf quantities at the angular frequency ω. Substituting these expressions into Equation 4, the internal field becomes

$$\vec{H} = \vec{H}_{dc} - \overleftrightarrow{N} \cdot \vec{M} + (\vec{h} - \overleftrightarrow{N} \cdot \vec{m})\epsilon^{j\omega t}. \tag{7}$$

The ac equation to determine the microwave susceptibility of the medium and to evaluate the resonance conditions can be found in its most general form by substituting Equations 5 and 7 into Equation 3 and expanding the resulting equation in terms of the exponential components. If $M_s >> m$ and $H_{dc} >> h$ and all terms of higher order than the first power in the small quantities $\vec{h}$ and $\vec{m}$ are neglected, this development is known as the linear or small-signal approximation. The dc equation also obtained from this expansion indicates that to the first order the internal dc field and the magnetization are in the same direction.

For arbitrarily oriented fields, the results obtained above are very involved expressions. In most practical cases, the dc magnetic field is applied parallel to one of the principal geometrical axes, say the z-axis, and the rf field $\vec{h}$ is usually applied in the x-y plane. Therefore the solution for arbitrarily oriented fields is not of great interest. The equation of motion of the magnetization vector determines the resonance conditions and also relates the rf magnetization vector to the microwave magnetic field vector.

1. Resonance conditions

The problem of determining the conditions of resonance in macroscopic samples of ferrimagnetic materials has been solved (19) and the result is embodied in Kittel's equation which neglects magnetic anisotropy and assumes the sample has been uniformly magnetized to saturation with the dc field applied parallel to the z-axis; i.e.,

$$(\omega/\gamma)^2 = [H_{dc} + (N_x - N_z)\, M_s]\, [H_{dc} + (N_y - N_z)\, M_s] \qquad (8)$$

where the parameters have been defined previously. This equation shows how complicated the resonance condition in a macroscopic sample is when compared to the free electron equation. The demagnetizing factors in Equation 8 depend only upon the geometry of the sample. If anisotropy is considered (particularly in the case of single-crystal materials), other factors related to crystal orientation must be introduced. The demagnetizing factors and resonance conditions for several idealized shapes are listed in Table 1 (20).

2. Susceptibility tensor

The vector relationship between the rf magnetization and the

Table 1. Demagnetizing factors and resonance conditions for ferrimagnetic resonators of idealized shape

Shape	Demagnetizing factor N_x	N_y	N_z	Resonance condition
Disc (H_{dc} normal)	0	0	1	$\gamma(H_{dc} - M_s)$
Sphere	1/3	1/3	1/3	γH_{dc}
Plane (H_{dc} parallel)	0	1	0	$\gamma[H_{dc}\ (H_{dc} + M_s)]^{1/2}$
Rod (H_{dc} parallel)	1/2	1/2	0	$\gamma(H_{dc} + M_s/2)$

microwave magnetic fields is usually expressed in terms of the susceptibility tensor $\overleftrightarrow{\chi}$ defined by

$$\vec{m} = \overleftrightarrow{\chi}_{ext} \cdot \vec{h}$$

$$= \begin{bmatrix} \chi_1 & -j\kappa & 0 \\ j\kappa & \chi_2 & 0 \\ 0 & 0 & 1 \end{bmatrix} \cdot \vec{h} \qquad (9)$$

In Equation 9, the rf magnetization vector has been related to the external microwave fields rather than the internal fields. Patel (7) has given the components of the external susceptibility tensor for a saturated ferrimagnetic sample of arbitrary shape as

$$\chi_1 = \frac{\omega_m[\omega_o + \omega_m(N_y - N_z) + j\omega\alpha] + \alpha^2\omega_m[\omega_o + \omega_m(N_y - N_z)]}{D}, \qquad (10)$$

$$\chi_2 = \frac{\omega_m[\omega_o + \omega_m(N_x - N_z) + j\omega\alpha] + \alpha^2\omega_m[\omega_o + \omega(N_x - N_z)]}{D}, \qquad (11)$$

$$\kappa = \frac{\omega_m \omega}{D} , \qquad (12)$$

where

$$D = [\omega_o + \omega_m(N_x - N_z) + j\omega\alpha][\omega_o + \omega_m(N_y - N_z) + j\omega\alpha]$$

$$-\omega^2 + \alpha^2\{\omega^2 + [\omega_o + \omega_m(N_x - N_z)][\omega_o + \omega_m(N_y - N_z)]\} ,$$

$\omega_o = \gamma H_{dc}$, $\omega_m = \gamma M_s$ and the dc magnetic bias has been directed along the z-axis. These expressions can easily be simplified by inserting the values of the demagnetizing factors for the particular ellipsoidal shape used. For a sphere,

$$\chi_1 = \chi_2 = \frac{\omega_o \omega_m}{\omega_o^2 - \omega^2 + 2j\omega\omega_o\alpha} \qquad (13)$$

and

$$\kappa = \frac{\omega\omega_m}{\omega_o^2 - \omega^2 + 2j\omega\omega_o\alpha} . \qquad (14)$$

B. Parameters of Ferrimagnetic Resonator Materials

In the previous section describing the ferrimagnetic resonance, a number of parameters were introduced. Several of these parameters and others related to them influence the practical application of ferrimagnetic resonators, therefore further discussion of their characteristics is warranted.

1. Saturation magnetization

The saturation magnetization M_s is a function of the number of electron spins in the material per unit volume and is defined as that net value of magnetization which corresponds to maximum alignment of all magnetic spins at a given temperature[2]. For yttrium-iron-garnet (YIG),

$4\pi M_S$ is 1750 gauss at room temperature (11). For lithium ferrite, $4\pi M_S$ is about 3550 gauss (14). If gallium is substituted into the crystal structure of YIG, $4\pi M_S$ may be varied from about 300 to 1750 gauss by controlling the doping level (11). Other forms of doping and materials are possible (21 thru 25). As will be shown later, it will be easier to couple to a material with a large M_S, but it may also restrict the lowest operating frequency.

2. Resonance conditions

The resonance conditions for the general ellipsoid, neglecting anisotropy, have been obtained from the Kittel equation and were presented earlier. The resonance frequency depends upon the applied field intensity and the shape dependent demagnetizing factors. Referring to Table 1, the resonance frequency of the sphere is the same as that of a free electron, while the rod cannot in theory resonate below a frequency determined by $\gamma M_S/2$. The lowest resonance frequency for a given external field is obtained by using a disc. Conversely, the disc requires a larger external field to obtain a given ferrimagnetic resonance frequency.

To tune a ferrimagnetic resonator to successively lower frequencies, the intensity of the applied field H_{dc} necessary to give resonance must be similarly reduced. When the applied field becomes so low as to be

---

[2]The most commonly used unit for saturation magnetization is the gaussian unit and is given as $4\pi M_S$ gauss. The value can be converted to MKS units by use of the conversion

M_S (in ampere-turns/meter) = 79.5 x $4\pi M_S$ (in gauss).

approximately equal to or less than the internal demagnetizing field, the resonator ceases to function. Since the internal demagnetizing field is determined by M_s and the geometric demagnetizing factors, the minimum resonant frequency is determined by the saturation magnetization and the resonator shape. For YIG the minimum resonance frequency for a spherical sample is about 1.63 gc/s. Although the shape of the resonator can have considerable effect on the resonance frequency, the sphere is generally the most practical since it is easiest to prepare with precision. A practical way to obtain lower minimum resonance frequencies is to use materials having a lower saturation magnetization such as Ga-YIG.

3. Phenomenological damping constant

The phenomenological damping constant α is a parameter introduced into the Landau-Lifshitz formulation of the equation of motion for the magnetization to account for losses. Its value at resonance is obtained from the expression (7)

$$\alpha = \frac{\gamma \Delta H}{2\omega_o} = \frac{\Delta H}{2 H_{dc}} , \qquad (15)$$

where ΔH is the line width of the magnetic sample. The line width appearing in this expression is defined in various ways, but basically it is the width of the ferrimagnetic resonance response obtained by holding the signal frequency constant and varying the applied dc field. Although the damping constant α will be used in this dissertation to simplify the mathematical format, the line width is a parameter used more frequently in practice because it can be obtained directly by measurement.

4. Line width

Ferrimagnetic resonance is determined experimentally by placing the ferrite material in a microwave cavity and observing the absorption of energy as the applied dc magnetic field is varied and the signal frequency is kept constant (26, 27, 28). Broadening of the resonance line (as it is called) is usually caused by interactions of the electron spins with each other and the crystal lattice. Therefore the line width may be affected by imperfections, inhomogeneity, strains, porosity, surface roughness, ionic substitutions and geometrical demagnetizing effects. The damping mechanisms are not fully understood and are the subject of much research.

Since there is greater lattice coupling in a single-crystal material as compared to a polycrystalline ferrite, the line width is narrower. The line width of polycrystalline YIG is about 40 to 50 oersteds, while the highly polished single-crystal YIG may have a line width of less than one oersted.

5. Unloaded Q

Associated with the ferrimagnetic resonance phenomenon is the parameter called unloaded Q(Q_u). Patel (7) has derived the formula for Q_u from the basic definition

$$Q_u = \omega_o \cdot \frac{\text{Energy stored in the sample}}{\text{Power lost in the sample}} . \qquad (16)$$

He assumed that the material was saturated by a field in the z direction and that $\vec{M}$ was uniform throughout the sample. For an ellipsoid of revolution about the z-axis, he obtained

$$Q_u = \frac{H_{dc} + (N_t - N_z)\, M_s}{\Delta H} \qquad (17)$$

where N_t is the transverse demagnetizing factor and N_z is the demagnetizing factor in the z direction. It can be seen that the unloaded Q of the resonator depends upon its line width, saturation magnetization and shape as well as the applied dc field. For a sphere where $N_t = N_z = 1/3$,

$$Q_u = \frac{H_{dc}}{\Delta H} = \frac{\omega_o}{\gamma \Delta H} . \qquad (18)$$

According to Carter and Flammer (29), the unloaded Q of YIG will increase with frequency up to about 5 to 10 gc/s, but then the curve of Q_u levels out. According to Douthett and Kaufman (30), useful Q's appear to be possible up to about 60 gc/s. In practice, the unloaded Q will be degraded by image currents flowing in metallic walls near the resonator.

6. Magnetic anisotropy and orientation of crystal axes

The only internal field opposing the external field which we have considered thus far has been that created by geometrical effects. Another source that can be treated as though it were another internal magnetic field arises from the anisotropy energy which causes preferential alignment of magnetic dipoles along certain crystalline directions. Because the material is easier to magnetize along some crystal axes than along others, the ferrimagnetic resonance frequency of the resonator will be influenced to some extent by the orientation of the crystal axes with respect to the biasing dc magnetic field.

Materials such as YIG and Ga-YIG have cubic crystalline structure and, therefore, have three sets of principal crystal axes as shown in Figure 6.

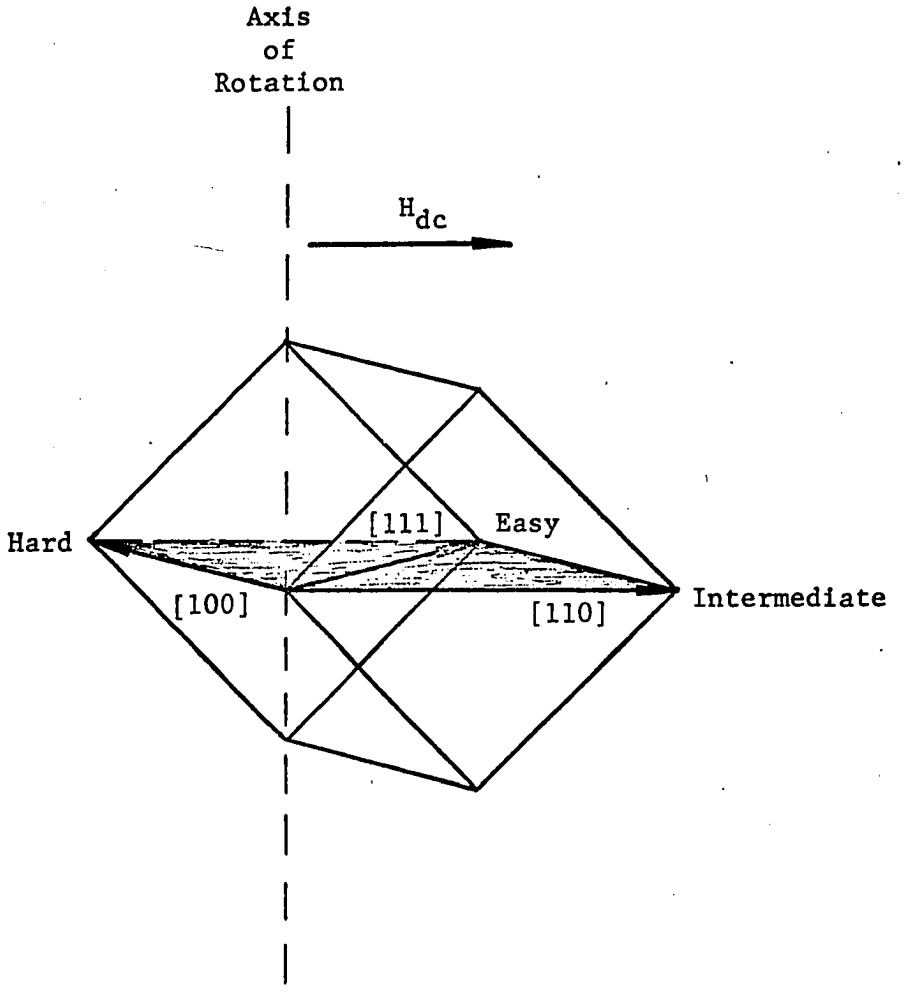

Figure 6. Directions of hard, easy and intermediate axes of magnetization for cubic crystal with negative anisotropy

There are three [100] axes, six [110] axes and four [111] axes in each single crystal. With a negative first-order anisotropy constant K_1/M_s, orientation of H_{dc} along the [111] axes of a sphere gives resonance at a lower field strength than that indicated in Table 1. Orientation along the [100] axes gives an intermediate effect. If K_1/M_s is positive, the role of the axes is reversed.

If a sphere of YIG is rotated about a [110] crystal axis that is perpendicular to H_{dc} as illustrated in Figure 6, the sphere at different times will have a [100], [110] or [111] axis parallel to H_{dc}. Since the field strength for resonance will cover all possible values as the resonator is rotated, this arrangement provides a practical means to compensate for the detuning effects of metallic boundaries, surface roughness, etc.

C. Higher-order Magnetostatic Modes

In the desired uniform precession resonance mode of ferrimagnetic resonators, all electron spins within the material precess with the same phase. However, higher-order modes, in which the phases of the precessions in parts of the resonator are different from the phases in other parts, can occur (31, 32). These higher-order modes cause the resonator to have more than one resonant frequency for a given intensity of biasing magnetic field. These phase differences between the spins may be caused by non-uniformity in either the applied biasing dc field or the microwave magnetic field. Since metallic boundaries are required near ferrimagnetic resonators in order to couple to them, disturbing effects which tend to excite higher-order magnetostatic modes are always present. Therefore

care must be exercised in the construction of the coupling structure to make the magnetic fields as uniform as possible.

Fletcher and Solt (33) found that the coupling to higher-order magnetostatic modes is related to the ratio of the diameter d of the sphere and the wavelength λ of the signal frequency. Reducing the ratio d/λ reduces the coupling to higher-order modes. Thus it is desirable to use ferrimagnetic resonators as small as possible consistent with obtaining adequate coupling to the external circuits at the uniform precession mode.

III. INVESTIGATION

Whereas a number of researchers have investigated band pass and band reject filters using YIG resonators in coaxial, stripline and waveguide structures, the input and output transmission lines have either been common (band reject) or constructed to minimize the coupling between the lines in the absence of the YIG (band pass). In the latter case, the fields of the input and output lines were orthogonal at the aperture between the two lines which contained the YIG. Due to the physical properties of the resonator, these band pass devices were non-reciprocal in the sense that the phase shift in one direction of propagation was +90° and in the other was -90°. If the input and output lines are common, the devices were non-reciprocal only if the magnetic fields were elliptically polarized.

The investigation here was concerned with a structure that will permit various degrees of coupling between the fields of the input and output lines. The coupling was controlled by an aperture in an iris diaphragm on the transverse cross-section of the transmission line. Since the transmission of electromagnetic energy between an antenna and receiver at the lower microwave frequencies is most commonly done with a coaxial cable, that geometry was chosen for study. It should be apparent that the results of this investigation can be extended to cover the other forms of microwave construction (stripline, waveguide, etc.).

A. Description of Coaxial Coupling Structures

The coupling structure which was investigated for this dissertation

was a coaxial configuration with an iris discontinuity. The purpose of investigating this form of structure was to obtain a controllable amount of coupling between the input and output transmission lines, while attempting to avoid some of the practical problems of mechanical design.

To minimize off-resonance coupling, most earlier investigators constructed their filters so that the fields in the input and output lines were orthogonal. This usually required the coupling structure to consist of shorted transmission lines crossed at the point of high magnetic field intensity. The ferrimagnetic resonator was placed at the intersection. If the transmission lines had a closed configuration (coaxial or waveguide), coupling between the two lines was accomplished by placing an aperture in the walls of the lines at the common point of intersection. Since the shorted lengths of line were multiples of one-half wavelength at the signal frequency, the structure was frequency sensitive. These shorted lengths of line and the crossed configuration tend to increase the physical dimensions of the structure and limit the flexibility in the design of the dc magnetic biasing arrangement. The coupling principle illustrated in Figure 3 eliminated the shorted sections of transmission line and that source of frequency dependence, but also tended to limit the flexibility in the design of the dc magnetic biasing arrangement. However, in all cases the coupling between the input and output transmission lines without the ferrimagnetic resonator was minimized.

The problem of design flexibility for the dc magnetic biasing arrangement appears to be unavoidable. However, the requirement to minimize coupling without the resonator seems to be too stringent in some

applications. Thus the effects of field coupling in addition to resonator coupling have been investigated.

Figure 7 is a sketch illustrating the geometry and construction of the coaxial coupling structure. A thin conducting iris perpendicular to the axis of the coaxial line contacts the inner and outer conductors. If the iris completely covers the surface of the cross-section, it represents a short circuit on the line and no energy will be propagated beyond the iris. To permit coupling, an aperture which may be of arbitrary shape is placed in the iris. As the area of this aperture increases, more and more energy at a given signal frequency passes through the iris, therefore the coupling between the input and output lines can be controlled by varying the size of the aperture.

The purpose of the YIG resonator is of course to provide another form of coupling between the input and output lines. To accomplish this the YIG is physically located in the aperture so that the plane of the iris intersects the center of the resonator, which for this investigation has been a sphere. The position of the sphere determines the amount of coupling between the magnetic fields of the microwave signal and the ferrimagnetic resonator. A dielectric support contains a tapped hole at a specified radial distance from the axis of the line. The sphere is attached to a dielectric screw by means of an epoxy adhesive, and can therefore be positioned with respect to the plane of the iris by rotating the screw.

The dc magnetic bias for the ferrimagnetic resonator is obtained by placing a solenoidal electromagnet about the entire structure. Since the

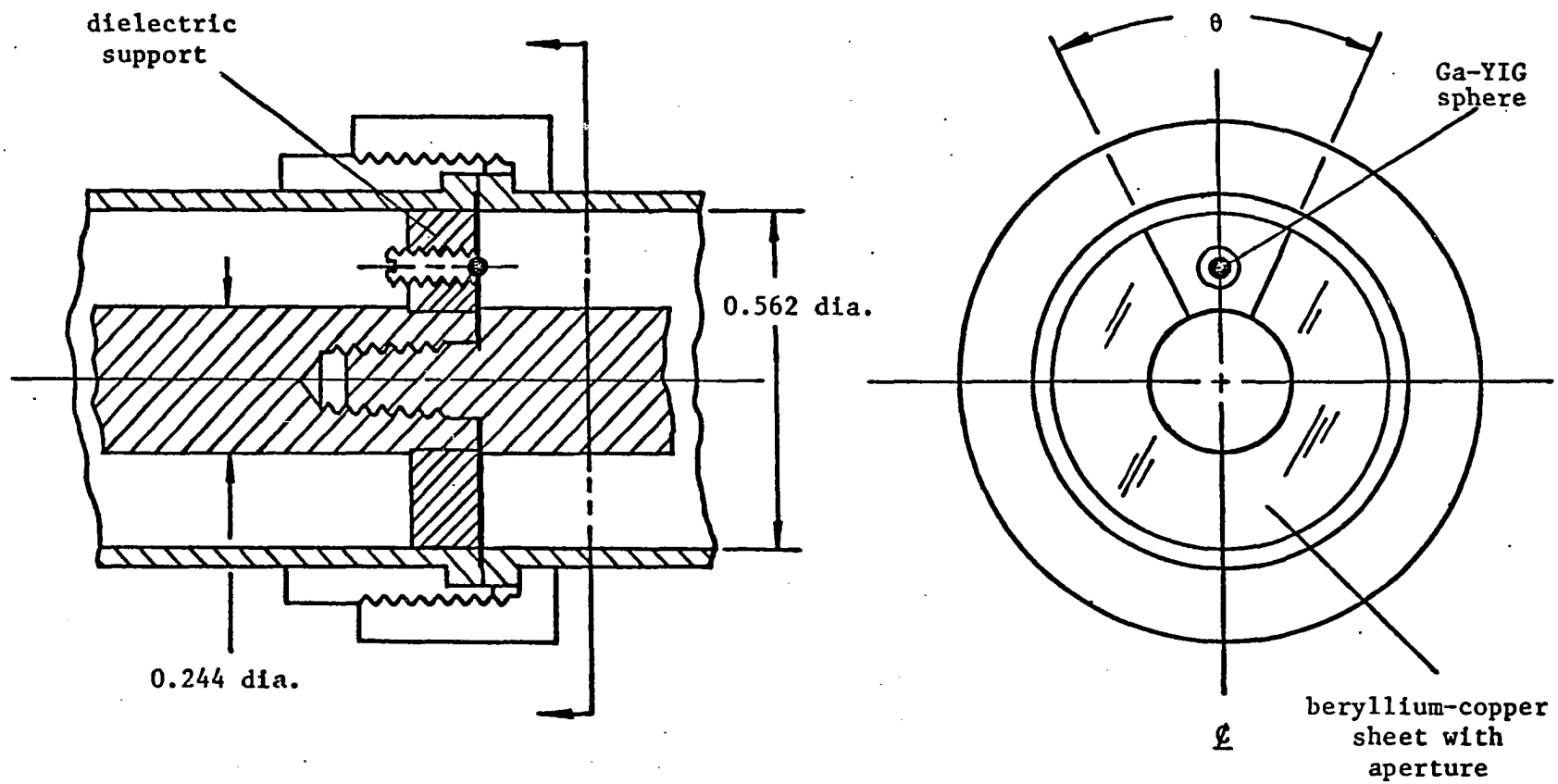

Figure 7. Coaxial line coupling structure for ferrimagnetic resonator

magnetic field intensity of the solenoid is uniform over its internal cross-section, the field applied to the ferrite sphere is independent of its position relative to the cross-section of the transmission line. The easy magnetization axis of the sphere is oriented with respect to the axis of the dielectric screw by placing it in a strong magnetic field during the application of the adhesive. In this way, the easy axis of the sphere is aligned parallel to the dc magnetic field.

The aperture in the iris is a pie-shaped sector cut from the ring contacting the inner and outer conductors of the coaxial line. The size of the angle containing the open sector determines the off-resonance coupling. Minimum coupling is represented by an aperture angle that is only large enough to clear the ferrite sphere. Maximum coupling is represented by complete elimination of the iris. This latter case is also the arrangement for a band reject filter.

B. Analytic Determination of Transmission Characteristics

The determination of the transmission characteristics of a coaxial line structure requires the solution of the scalar Helmholtz equation in cylindrical polar coordinates (34). In general the field solutions contain a TEM wave and higher-order TE and TM modes. The wavelengths of the higher-order modes are related to the radial dimensions of the line. Therefore, if the dimensions of the line are small compared to the principal wave length, the fields of these higher-order modes will decay rapidly.

Since in practice the dimensions are selected so that the higher-order modes do not propagate, the problem is simplified by considering

only the TEM mode to exist. The YIG spheres normally used are indeed small relative to the dominant mode in the line, but their response to the propagating wave is very strong due to their high Q. By utilizing the external tensor of magnetic susceptibility, the higher oscillation modes near the YIG sphere will be accounted for by means of the demagnetizing form factors.

To determine the transmission characteristics for the coaxial structure described above, we will assume that the total field within the line consists of the superposition of all fields; i.e., it will consist of the incident field on the line, the reflected field from the iris and the excitation field of the magnetic dipole source in the sphere. We will also assume that the walls of the line are perfect conductors. The analysis will be carried out in three steps and is applicable to all materials that exhibit ferrimagnetic resonance.

1. An approach to the determination of iris characteristics without YIG using insertion loss data

The equivalent circuits for numerous forms of geometric discontinuities in transmission lines have been developed by Schwinger, Levine, and others (35). The equivalent circuits were derived using approximate perturbation, variational or integration methods. In general the equivalent circuit for a lossless discontinuity in a transmission line is a Π or T reactance network. If the discontinuity is a thin iris whose thickness is very much less than a wavelength at the signal frequency, the equivalent circuit reduces to a single shunt reactance which will be either inductive or capacitive depending upon the field configurations

required to satisfy the boundary conditions. For an iris connecting the inner and outer conductors of a coaxial line, the reactance is inductive and the equivalent circuit for an infinite line becomes that shown in Figure 8. Using this equivalent circuit, the power transmitted to the load can be determined by straight-forward transmission line analysis techniques.

Since the infinite transmission line beyond the discontinuity is equivalent to a matched line, the transmission line between the generator and X_o is terminated by the parallel combination of an inductive reactance jX_o and the characteristic impedance Z_o. Assuming that the characteristic impedance is real, the terminating impedance is

$$Z_L = \frac{jX_o Z_o}{Z_o + jX_o} \quad . \tag{19}$$

The current reflection coefficient, which is the negative of the voltage reflection coefficient, is defined as

$$\rho_o = \frac{Z_o - Z_L}{Z_L + Z_o} \tag{20}$$

and for this termination becomes

$$\rho_o = \frac{Z_o}{Z_o + j2X_o} \quad . \tag{21}$$

The standing wave ratio of the transmission line is defined as

$$S = \frac{1 + |\rho_o|}{1 - |\rho_o|} \quad . \tag{22}$$

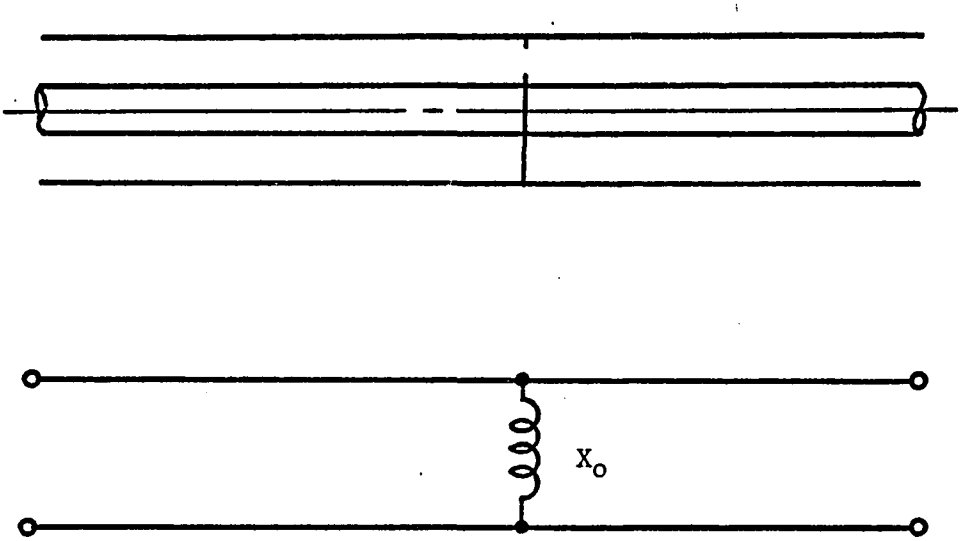

Figure 8. Equivalent circuit for an iris in a coaxial transmission line

It is a real number greater than unity and upon substitution for ρ_o becomes

$$S = \frac{(Z_o^2 + 4X_o^2)^{1/2} + Z_o}{(Z_o^2 + 4X_o^2)^{1/2} - Z_o} \quad . \tag{23}$$

The ratio of the power in the load to the power incident on the line is defined as

$$|T_o|^2 = \frac{4S}{(1 + S)^2} \quad , \tag{24}$$

where T_o is the transmission coefficient. It also can be solved in terms of the magnitude of the shunt reactance and the characteristic impedance of the line:

$$|T_o|^2 = \frac{4X_o^2}{Z_o^2 + 4X_o^2} \quad . \tag{25}$$

Using this expression, it is possible to solve for X_o in terms of $|T_o|^2$ and Z_o:

$$X_o = \pm \frac{Z_o}{2} \left[\frac{|T_o|^2}{1 - |T_o|^2}\right]^{1/2} \quad . \tag{26}$$

Since $|T_o|^2 \leq 1$ the finite magnitude of the reactance X_o is always real. The character of the reactance, capacitive or inductive, has been lost in this analysis, but it was understood to be inductive. The power ratio $|T_o|^2$ can be measured experimentally with relative ease. Therefore, we will define the reciprocal of $|T_o|^2$ as the initial attenuation α_o and use this parameter in subsequent analytical evaluations rather than calculate the equivalent shunt reactance.

2. The ferrimagnetic resonator in an infinite coaxial line without iris discontinuity

In examining the interaction between a ferrite and a transmission line, either of two approaches may be used: (1) Solve the boundary value problem relating the magnetic permeability of the ferrite to the frequency ω and the constant internal field H_{io} in a given form, or (2) treat the variable magnetization of the ferrite as a whole to be a coupled resonant system. The first approach is useful in a limited number of cases and usually leads to complicated calculations. The treatment of the ferrite as a resonant system coupled to other resonant systems has been developed by Bloembergen and Pound (36). Most subsequent contributions calculate the parameters of the small ferrite ellipsoid on the latter basis because it usually does not lead to mathematical difficulties. Maslennikova (37) solved the problem of a magnetized ferrite sphere placed in the field of a TEM-mode transmission line utilizing a general electrodynamic method developed by Gurevich (38) which determines the reflection and transmission coefficients of the line with the sphere present. A similar solution will be presented here, then the method will be extended to apply to the coaxial transmission line with an iris discontinuity.

The method of Gurevich considers the variable magnetization of the ellipsoid to be a resonant system which is exciting an electromagnetic field (radiation field) in the transmission line and at the same time is being excited by a "self-consistent" field made up of the unperturbed field $\vec{h}_e$ of the line and this radiation field $\vec{h}_r$. The magnetization of the sphere is related to these two fields by the external magnetic

susceptibility tensor of the ferrite $\overleftrightarrow{\chi}$ as follows

$$\vec{m} = \overleftrightarrow{\chi} (\vec{h}_e + \vec{h}_r). \tag{27}$$

The problem is solved by first calculating the radiation field excited in the line by a variable magnetization source $\vec{m}(t) = \vec{M}_s \varepsilon^{j\omega t}$ concentrated in the volume of the sphere, and then calculating the magnetization of the sphere caused by the unperturbed and radiation fields. In the remainder of this dissertation, time-independent field amplitudes will be symbolized by capital letters.

a. Radiation field The excitation of the fields in a lossless coaxial transmission line by a given intensity of magnetization can be found by solving the scalar Helmholtz equation

$$\frac{1}{\rho} \frac{\partial}{\partial \rho} \left(\frac{\partial H}{\partial \rho} \right) + \frac{1}{\rho^2} \frac{\partial^2 H}{\partial \phi^2} + \frac{\partial^2 H}{\partial z^2} + k^2 H = M \tag{28}$$

in cylindrical polar coordinates (ρ, ϕ, z) and applying the boundary conditions that the normal derivatives of H vanish at all conducting surfaces. However, the fields of the TEM mode are well known so it will be more convenient to determine the effective coupling of the ferrite by starting with these known fields.

Referring to Figure 9, we know that a radiated TEM mode propagating to the right of the sphere consists of a single transverse magnetic component described by

$$\vec{H}_{rad} \varepsilon^{-jkz} = H_\phi \varepsilon^{-jkz} \hat{e}_\phi = \frac{I}{2\pi\rho} \varepsilon^{-jkz} \hat{e}_\phi \tag{29}$$

where I is the total current flowing in the center conductor, ρ is the radial distance from the center of the line and $\hat{e}_\phi$ is the unit vector in the ϕ direction. Since the fields satisfy Maxwell's equations except in

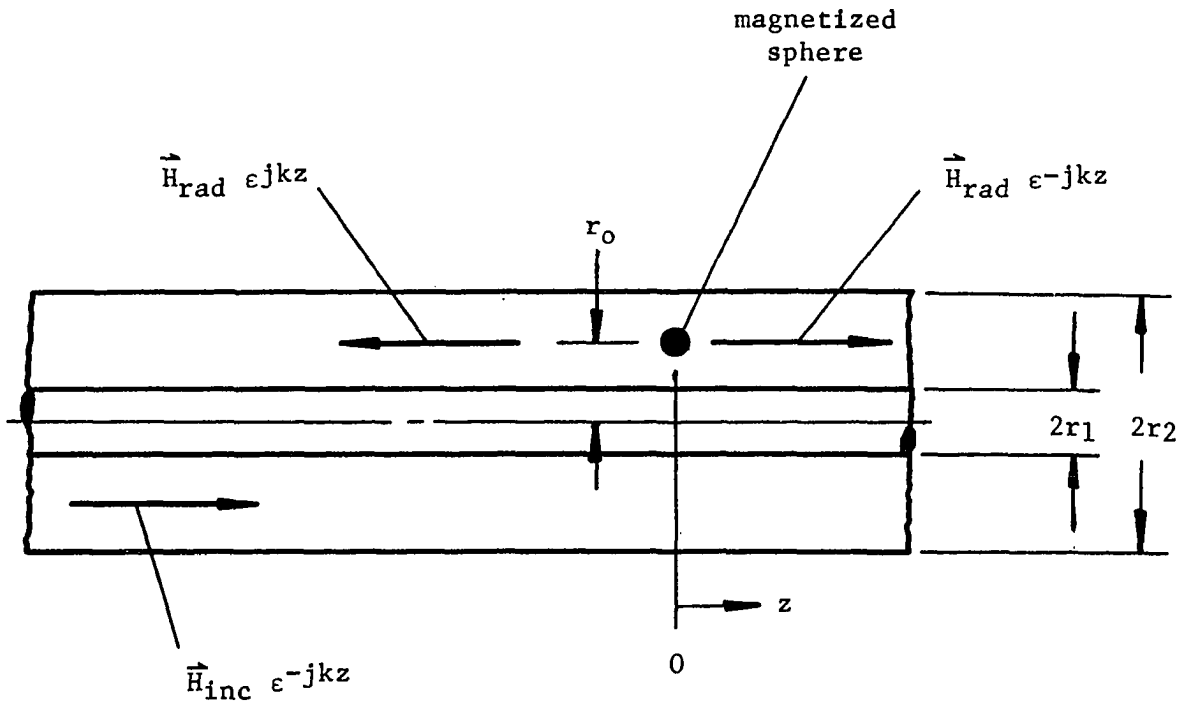

Figure 9. Field configurations for coaxial line without iris

the plane containing the sphere, the electric field is

$$\vec{E}_{rad}\, \epsilon^{-jkz} = \eta_o(\vec{H}_{rad} \times \hat{e}_z)\epsilon^{-jkz} = \frac{\eta_o I}{2\pi\rho}\, \epsilon^{-jkz}\, \hat{e}_\rho \tag{30}$$

where η_o is the characteristic impedance of free space, $\hat{e}_z$ is the unit vector in the z direction and $\hat{e}_\rho$ is the unit vector in the ρ direction.

The power propagating down the line can be determined by means of the Poynting vector,

$$\vec{P}_{rad} = 1/2\ \mathrm{Re} \int_s (\vec{E}_{rad} \times \vec{H}^*_{rad})\ ds \tag{31}$$

where $\vec{H}^*_{rad}$ is the complex conjugate of $\vec{H}_{rad}$ and s is the cross-sectional area of the coaxial line. Solving for $\vec{P}_{rad}$:

$$\begin{aligned}\vec{P}_{rad} &= 1/2\ \mathrm{Re} \int_0^{2\pi}\int_{r_1}^{r_2} \left[\frac{\eta_o I}{2\pi\rho}\, \hat{e}_\rho\right] \times \left[\frac{I}{2\pi\rho}\, \hat{e}_\phi\right]^* \rho d\rho d\phi \\ &= \frac{\eta_o I^2}{4\pi}\ (\ln r_2/r_1)\ \hat{e}_z \\ &= \frac{Z_o I^2}{2}\ \hat{e}_z \end{aligned} \tag{32}$$

since the characteristic impedance of a coaxial line is $\eta_o(\ln r_2/r_1)/2\pi$.

We may also express the power of this field incident to the right as

$$\vec{P}_{rad} = K_o(\vec{H}_o \cdot \vec{H}_o^*)\hat{e}_z, \tag{33}$$

where H_o is the magnitude of the magnetic field component at the position of the sphere without the resonator and K_o is a coupling constant given by the structure and the position of the sphere. Since at this point

$$\vec{H}_o = \frac{I}{2\pi r_o}\, \hat{e}_\phi, \tag{34}$$

the power in the radiation field is

$$\vec{P}_{rad} = \frac{K_o I^2}{4\pi^2 r_o^2} \hat{e}_z = \frac{Z_o I^2}{2} \hat{e}_z \qquad (35)$$

from which we can determine the coupling constant K_o,

$$K_o = 2\pi^2 Z_o r_o^2 \ . \qquad (36)$$

Now it is necessary to relate the strength of the radiated TEM mode to the magnetic dipole of the sphere. Since the reciprocity principle permits us to interchange the role of the source between the magnetization of the sphere and the TEM field, we may write the power coupled to the sphere by the radiation field as

$$\vec{P}_{rad} = - j\omega\mu_o \, v_f \, \vec{M} \cdot \vec{H}_{rad} \, \hat{e}_z \ , \qquad (37)$$

where the total magnetic dipole moment in the volume v_f has been assumed to be contained at the point $(r_o, 0, 0)$. We also assume that the dimensions of the sphere are sufficiently small so that the ferrimagnetic material is uniformly magnetized. Thus, if we consider a new Cartesian coordinate system (x', y', z') with its origin at the center of the sphere, its z'-axis parallel with the axis of the transmission line and its y'-axis parallel with the transverse radial vector from the center of the transmission line through the center of the sphere, only the x component of the magnetization will couple to a TEM magnetic field (see Figure 10). Therefore, Equation 37 becomes

$$\vec{P}_{rad} = \ j\omega\mu_o \, v_f \, M_x \, H_{rad} \, \hat{e}_z \ . \qquad (38)$$

It is now possible to determine the amplitude of the TEM field excited by the magnetization of the sphere by means of Equations 33, 36 and 38:

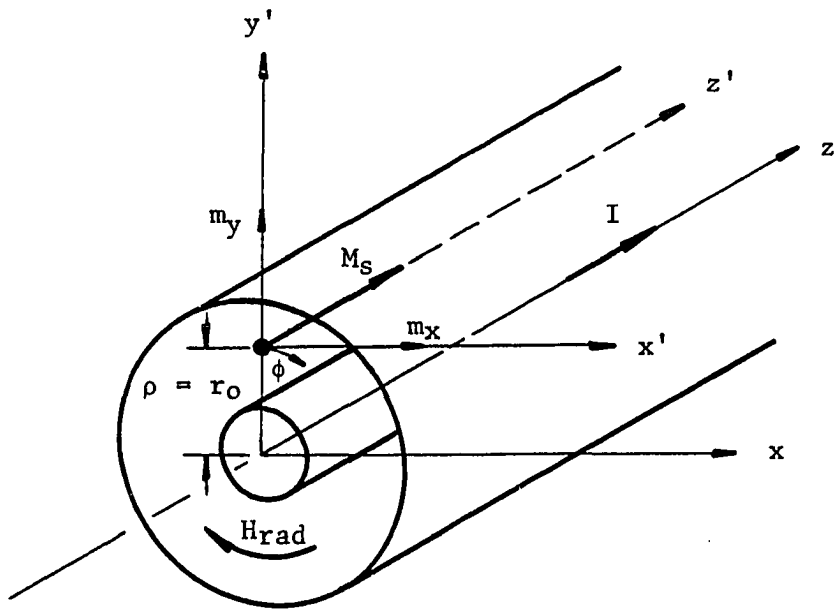

Figure 10. Coordinate systems used to determine radiation field excited by ferrimagnetic resonator in a coaxial transmission line

$$\vec{P}_{rad} = K_o(\vec{H}_{rad} \cdot \vec{H}^*_{rad})\hat{e}_z = j\omega\mu_o v_f M_x H_{rad} \hat{e}_z$$

$$K_o H_{rad} = - j\omega\mu_o v_f M_x$$

$$H_{rad} = \frac{- j\omega\mu_o v_f M_x}{K_o}$$

$$= \frac{- j\omega\mu_o v_f M_x}{2\pi^2 r_o^2 Z_o} \qquad (39)$$

Letting the parameter

$$a = \frac{\mu_o v_f}{2\pi^2 r_o^2 Z_o} , \qquad (40)$$

the radiation field can be expressed as

$$H_{rad} = - j\omega a M_x . \qquad (41)$$

By a similar procedure it is possible to show that there is a like radiation field propagating to the left of the sphere.

Having determined the radiation fields excited by the magnetization of the ferrite, it is now possible to find the reflection and transmission coefficients and thus the filter characteristics of the band reject configuration.

b. Reflection coefficient Referring to Figure 9, the reflection coefficient Γ is specified by the formula

$$\Gamma = \frac{H_{rad}\, \epsilon^{jkz}}{H_{inc}\, \epsilon^{-jkz}} = \frac{H_{rad}}{H_{inc}}\, \epsilon^{j2kz} , \qquad (42)$$

where $k = 2\pi/\text{wavelength}$ is the wave number.

From Equations 41 and 27,

$$H_{rad} = - j\omega a M_x = - j\omega a \chi_1 (H_{inc} + H_{rad})$$

so that

$$\frac{H_{rad}}{H_{inc}} = \frac{- j\omega a\chi_1}{1 + j\omega a\chi_1} \quad , \tag{43}$$

therefore,

$$\Gamma = \frac{- j\omega a\chi_1}{1 + j\omega a\chi_1} \varepsilon^{j2kz} \quad . \tag{44}$$

With the dc magnetic bias field applied in the +z direction, the diagonal component of the susceptibility tensor for a ferrite sphere is given by Equation 17,

$$\chi_1 = \frac{\omega_m \omega_o}{\omega_o^2 - \omega^2 + j2\omega\omega_o\alpha} \quad . \tag{17}$$

Substituting this expression into Equation 44 above, we obtain for the reflection coefficient

$$\Gamma = \frac{- j\omega a\omega_m\omega_o}{\omega_o^2 - \omega^2 + j\omega\omega_o(2\alpha + a\omega_m)} \varepsilon^{j2kz} \quad . \tag{45}$$

c. Transmission coefficient The transmission coefficient T for the band reject configuration is specified by the formula

$$T = \frac{(H_{rad} + H_{inc})\varepsilon^{-jkz}}{H_{inc}\ \varepsilon^{-jkz}} = 1 + \frac{H_{rad}}{H_{inc}} \quad . \tag{46}$$

If we substitute Equation 43 for the ratio, the transmission coefficient becomes

$$T = \frac{1}{1 + j\omega a\chi_1} \quad . \tag{47}$$

Equations 44 and 47 correspond to those developed for the band reject filter by Maslennikova (37). To obtain the complete expression it is once again necessary to substitute for χ_1. Thus, the final form for the transmission coefficient becomes

$$T = \frac{\omega_o^2 - \omega^2 + j2\omega\omega_o\alpha}{\omega_o^2 - \omega^2 + j\omega\omega_o(2\alpha + a\omega_m)} . \qquad (48)$$

The attenuation α_r, which we will define as the reciprocal of $|T|^2$, can then be expressed as

$$\alpha_r = \frac{(\omega_o^2 - \omega^2)^2 + \omega^2\omega_o^2(2\alpha + a\omega_m)^2}{(\omega_o^2 - \omega^2)^2 + 4\omega^2\omega_o^2\alpha^2} . \qquad (49)$$

Assuming that this expression describes the characteristics of the filter for all frequencies, we can determine whether the filter is truly band reject by some rather simple tests. If $\omega << \omega_o$ or $\omega >> \omega_o$, the value of the expression approaches unity so there is no attenuation through the filter. However, at ferrimagnetic resonance $\omega = \omega_o$ and the expression reduces to

$$\alpha_r\Big|_{\omega = \omega_o} = (1 + a\omega_m/2\alpha)^2 . \qquad (50)$$

Combining Equations 15 and 18, we find that $\alpha = 1/2Q_u$. Therefore, substituting for α and a, the attenuation at resonance becomes

$$\alpha_r\Big|_{\omega = \omega_o} = \left(1 + \frac{\mu_o v_f \omega_m Q_u}{\pi^2 r_o^2 Z_o}\right)^2 . \qquad (51)$$

This expression is always greater than one, so the filter will indeed provide a band reject characteristic.

Equation 51 also provides a quantitative description of how the various parameters of the sphere and coupling structure influence the attenuation at resonance. Increasing the volume of the sphere, the saturation magnetization or unloaded Q will increase the attenuation, while increasing the radial position of the sphere or the characteristic impedance of the line will decrease the attenuation. The freedom of choice

that we can actually exercise will depend upon the frequency range and practical limitations of mechanical design.

3. The ferrimagnetic resonator in an infinite coaxial line with iris discontinuity

The analysis of a ferrimagnetic resonator in an infinite coaxial line with an iris discontinuity follows the same method as the previously analyzed system without a discontinuity, but in this case the analysis must also take into consideration the field reflected from the conducting iris. As before, we will assume that only a TEM wave is propagated. To simplify the analysis, we will consider the sphere to be symmetrically located in the center of the aperture.

a. Radiation field First, let us consider the reflection and transmission coefficients for the structure without the ferrimagnetic resonator. Referring to Figure 11, the reflection coefficient in this case is

$$\Gamma' = \frac{H_{refl}\ \epsilon^{jkz}}{H_{inc}\ \epsilon^{-jkz}} = \frac{H_{refl}}{H_{inc}}\ \epsilon^{j2kz} = \rho_o \epsilon^{j2kz}, \tag{52}$$

where H_{refl} is the field reflected from the discontinuity, H_{inc} is the incident field and ρ_o is the reflection coefficient defined in Equation 20 and determined by Equation 21.

The transmission coefficient is

$$T' = \frac{H_{feed}\ \epsilon^{-jkz}}{H_{inc}\ \epsilon^{-jkz}} = \frac{H_{feed}}{H_{inc}}\ . \tag{53}$$

Since the field feeding through the aperture H_{feed} is the difference between the incident and reflected fields on the source side of the aperture, it is expressed as

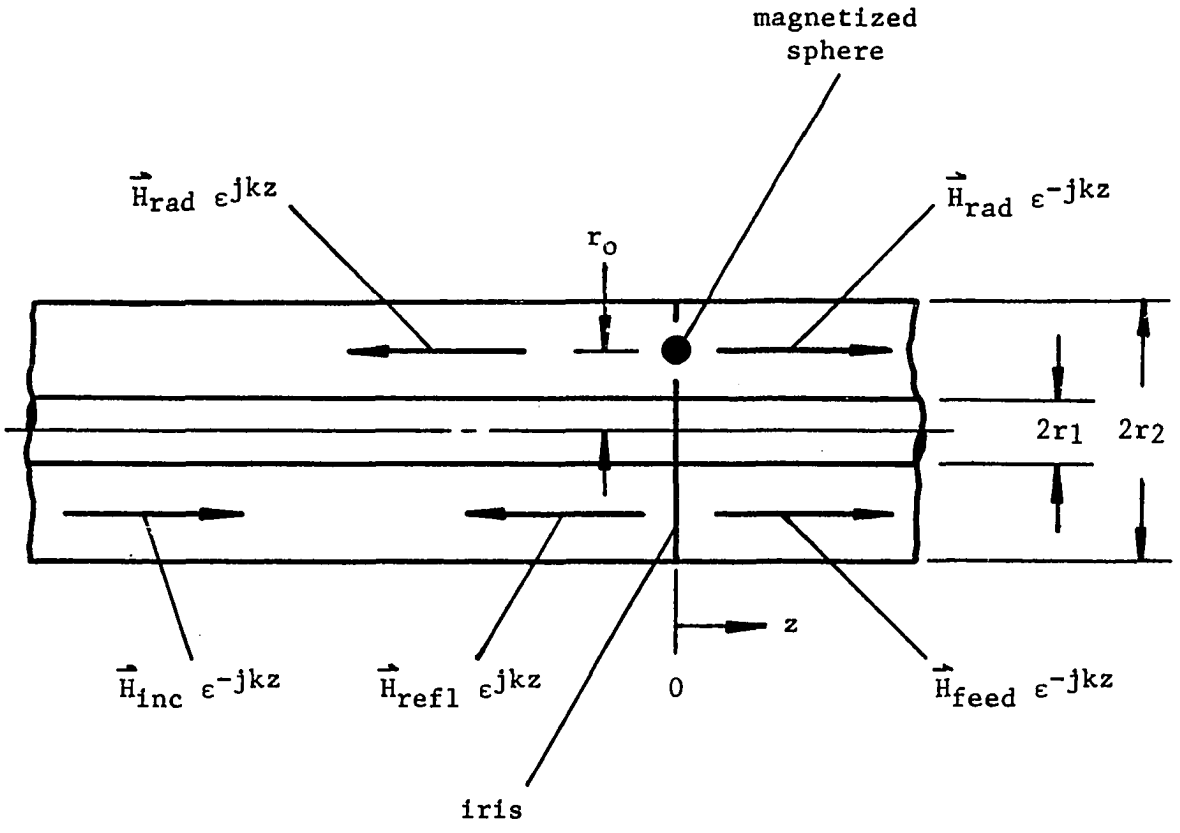

Figure 11. Field configuration for coaxial line with iris discontinuity

$$T' = \frac{H_{inc} - H_{refl}}{H_{inc}} = 1 - \frac{H_{refl}}{H_{inc}}$$

$$= 1 - \rho_o. \tag{54}$$

When the magnetized sphere is placed in the aperture of the iris, we assume as before that the total field is a superposition of the component fields without the resonator and the radiation fields excited by the resonator. However, the fields coupling to the magnetization of the sphere are more complex than those of the band reject filter. Since the plane of the iris bisects the resonator, the magnetic fields in each half of the sphere are not the same. The incident field, reflected field and radiation field couple to the left hemisphere (in Figure 11), while the feedthrough field and radiation field couple to the right hemisphere. At the bisecting plane the magnetic fields are continuous. If the resonator is small, we may assume that the exchange forces within the sphere are sufficiently strong to keep all microscopic magnetic dipoles aligned so that the approximate total coupling to the resonator is the sum of all field contributions. Then, the magnetization becomes

$$M_x = \underbrace{\frac{\chi_1}{2}(H_{inc} + H_{refl} + H_{rad})}_{\text{left half}} + \underbrace{\frac{\chi_1}{2}(H_{feed} + H_{rad})}_{\text{right half}}$$

$$= \chi_1 (H_{inc} + H_{rad}). \tag{55}$$

The radiation field, which is obtained by using Equation 41, becomes

$$H_{rad} = - j\omega a M_x$$

$$= \frac{- j\omega a \chi_1}{1 + j\omega a \chi_1} H_{inc} \tag{56}$$

and is the same as the radiation field for the band reject configuration. It is readily apparent that this result would not have been obtained if the sphere were not centered in the aperture. We can now proceed to the determination of the reflection and transmission coefficients for this structure.

b. Reflection coefficient The reflection coefficient for the resonator configuration with an iris is specified by the formula

$$\Gamma = \frac{(H_{refl} + H_{rad})\ \varepsilon^{jkz}}{H_{inc}\ \varepsilon^{-jkz}} = \frac{H_{refl}}{H_{inc}} + \frac{H_{rad}}{H_{inc}}\ \varepsilon^{j2kz}. \tag{57}$$

By substituting Equations 52 and 56, it becomes

$$\Gamma = \frac{\rho_o - j(1 - \rho_o)\omega a\chi_1}{1 + j\omega a\chi_1}\ . \tag{58}$$

If $\rho_o = 0$, which would correspond to the case of an infinite line without a discontinuity, the reflection coefficient reduces to Equation 44 which describes the band reject filter.

c. Transmission coefficient The transmission coefficient for the iris configuration is specified by the formula

$$T = \frac{(H_{feed} + H_{rad})\ \varepsilon^{-jkz}}{H_{inc}\ \varepsilon^{-jkz}}$$

and by similar substitutions as before becomes

$$T = \frac{1 - \rho_o(1 + j\omega a\chi_1)}{1 + j\omega a\chi_1}\ . \tag{59}$$

If $\rho_o = 0$, the transmission coefficient reduces, as expected, to Equation 47 and describes the band reject filter. Substituting for χ_1 and ρ_o,

$$T = \frac{\left(1 - \frac{Z_o}{Z_o + 2jX_o}\right)\left(1 + \frac{ja\omega_o\omega_m\omega}{\omega_o^2 - \omega^2 + 2j\omega\omega_o\alpha}\right)}{1 + \frac{ja\omega_o\omega_m\omega}{\omega_o^2 - \omega^2 + 2j\omega\omega_o\alpha}}$$

$$= \frac{-4X_o\omega\omega_o\alpha + j[2X_o(\omega_o^2 - \omega^2) - Z_o a\omega_o\omega_m\omega]}{(Z_o + 2jX_o)[\omega_o^2 - \omega^2 + j\omega_o\omega(a\omega_m + 2\alpha)]} . \qquad (60)$$

Therefore, the attenuation of the coaxial structure with an iris is described by

$$\alpha_r = \frac{\left| [Z_o(\omega_o^2 - \omega^2) - 2X_o\omega\omega_o(a\omega_m + 2\alpha)]^2 + [2X_o(\omega_o^2 - \omega^2) + Z_o\omega_o\omega(a\omega_m + 2\alpha)]^2 \right|}{16X_o^2\omega^2\omega_o^2\alpha^2 + [2X_o(\omega_o^2 - \omega^2) - Z_o a\omega\omega_o\omega_m]^2} . \qquad (61)$$

The behavior of Equation 61 as frequency is varied is somewhat more complex than the behavior displayed by Equation 49, but a few simple observations are possible. If $\omega << \omega_o$ or $\omega >> \omega_o$, the equation is asymptotic to

$$\alpha_r \Big|_{\omega << \omega_o} \simeq \alpha_r \Big|_{\omega >> \omega_o} \simeq \frac{Z_o^2 + 4X_o^2}{4X_o^2} , \qquad (62)$$

which is simply the attenuation of the transmission line and iris without a resonator; i.e., it is the reciprocal of Equation 25. If X_o is small, the attenuation is very large. At $\omega = \omega_o$, Equation 61 becomes

$$\alpha_r \Big|_{\omega = \omega_o} = \frac{(Z_o^2 + 4X_o^2)(a\omega_m + 2\alpha)^2}{16X_o^2\alpha^2 + Z_o^2 a^2 \omega_m^2} , \qquad (63)$$

which indicates that the attenuation at resonance is determined by the iris reactance as well as the sphere and transmission line

characteristics. If $a\omega_m$ and 2α are of the same order of magnitude and $X_o << Z_o$, the expression further reduces to

$$\alpha_r \Big|_{\substack{\omega = \omega_o \\ X_o << Z_o}} = (1 + 2\alpha/a\omega_m)^2 , \qquad (64)$$

which is independent of X_o. Since Equation 62 shows the attenuation far from resonance to be very high for small X_o and Equation 64 shows the attenuation to be much less at resonance, the filter displays a band pass characteristic. On the other hand, if $X_o >> Z_o$, Equation 63 simplifies to the band reject expression of Equation 50. The second term of Equation 64 is the reciprocal of the second term of Equation 50, therefore, the conditions that increased the resonance attenuation for the band reject filter will decrease the resonance attenuation, or insertion loss, for the band pass filter. Both results are consistent with conventional filter theory.

To examine in detail the character of the band pass expression for a range of frequencies near ferrimagnetic resonance and a number of parameter variations, Equation 61 was programmed for solution by means of an IBM 7074 computer and plotted by means of an S-C 4020 computer recorder. The results obtained are presented in Figures 12 through 19. Lines between the computer generated dots were drawn manually. In all cases the saturation magnetization $4\pi M_s$, which appears implicitly in ω_m, was 1040 gauss and the characteristic impedance Z_o of the line was 50 ohms. Attenuation was plotted on a logarithmic or decibel scale.

In Figure 12, the attenuation of the structure as a function of frequency deviation away from the ferrimagnetic resonance frequency of

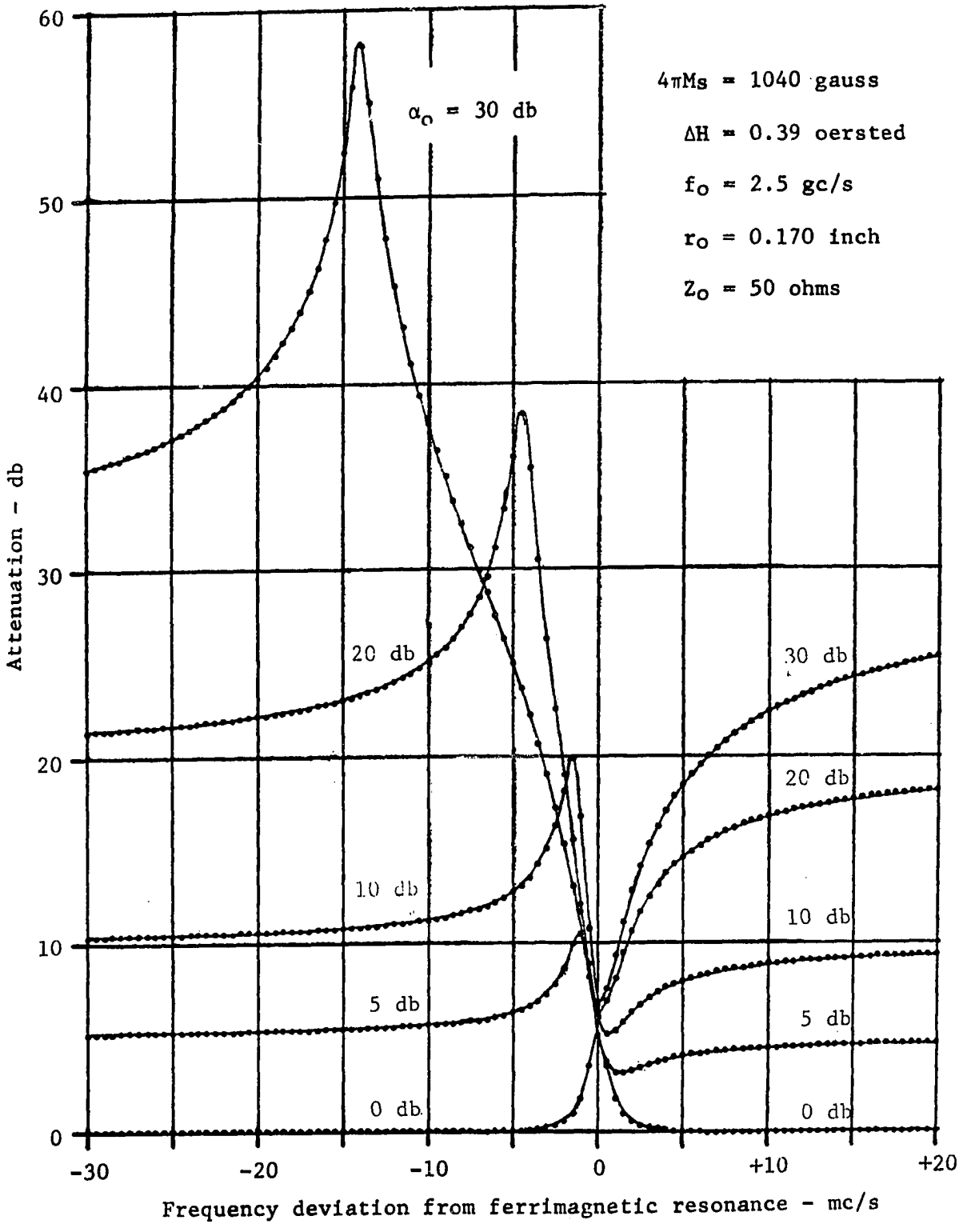

Figure 12. Computer solutions to Equation 61 for various values of initial attenuation

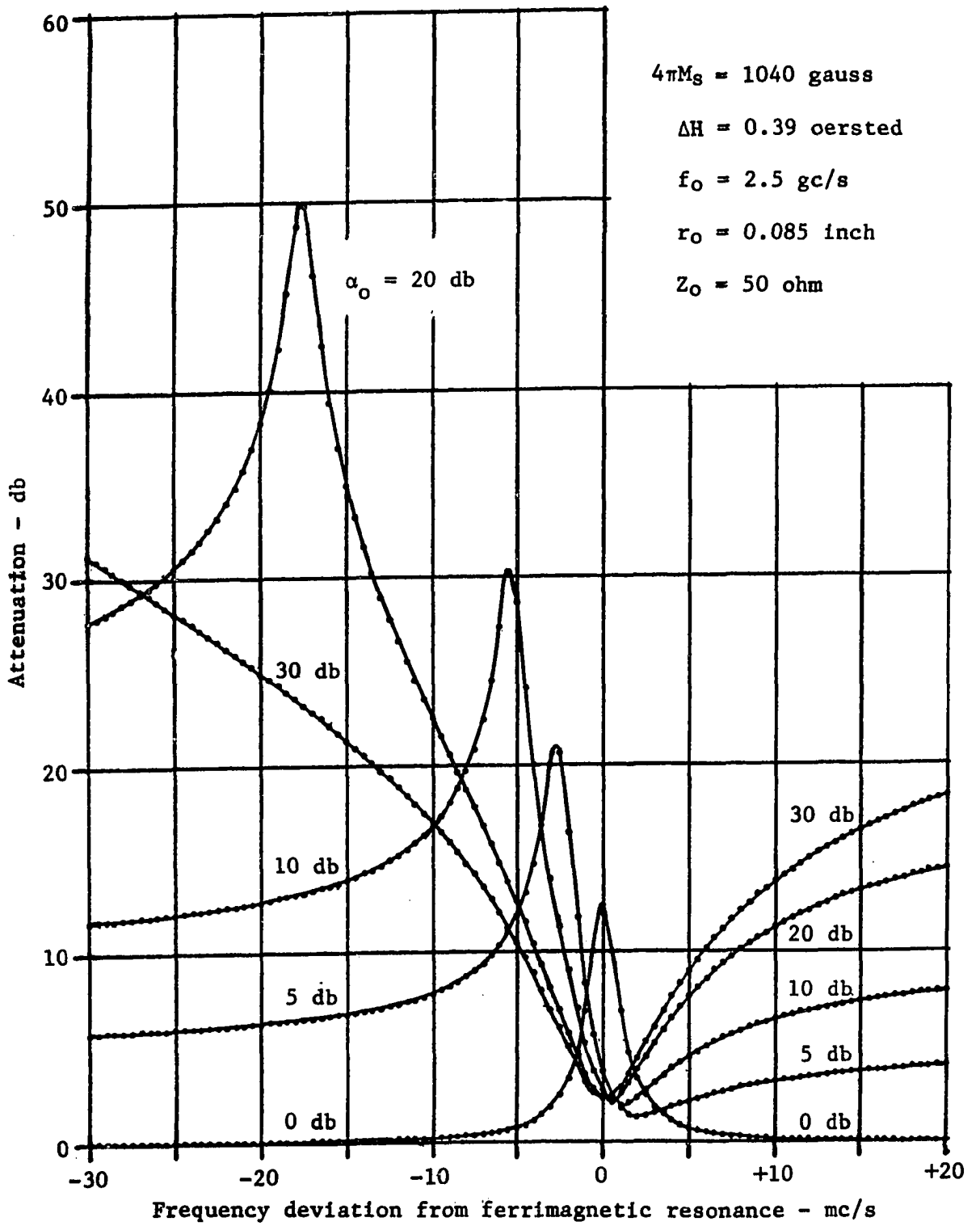

Figure 13. Computer solutions to Equation 61 with tighter coupling than the results shown in Figure 12

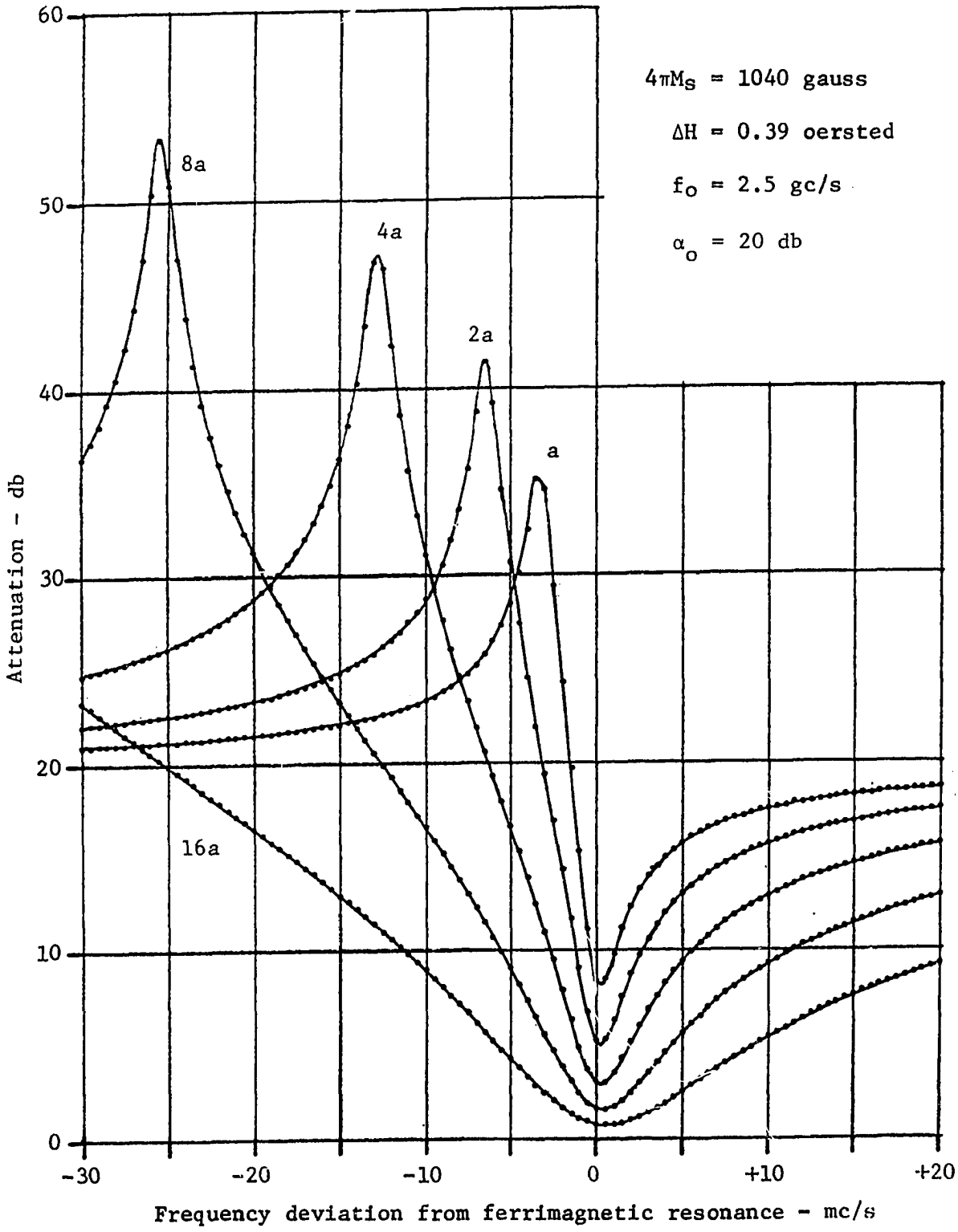

Figure 14. Computer solutions to Equation 61 for various values of the coupling parameter a

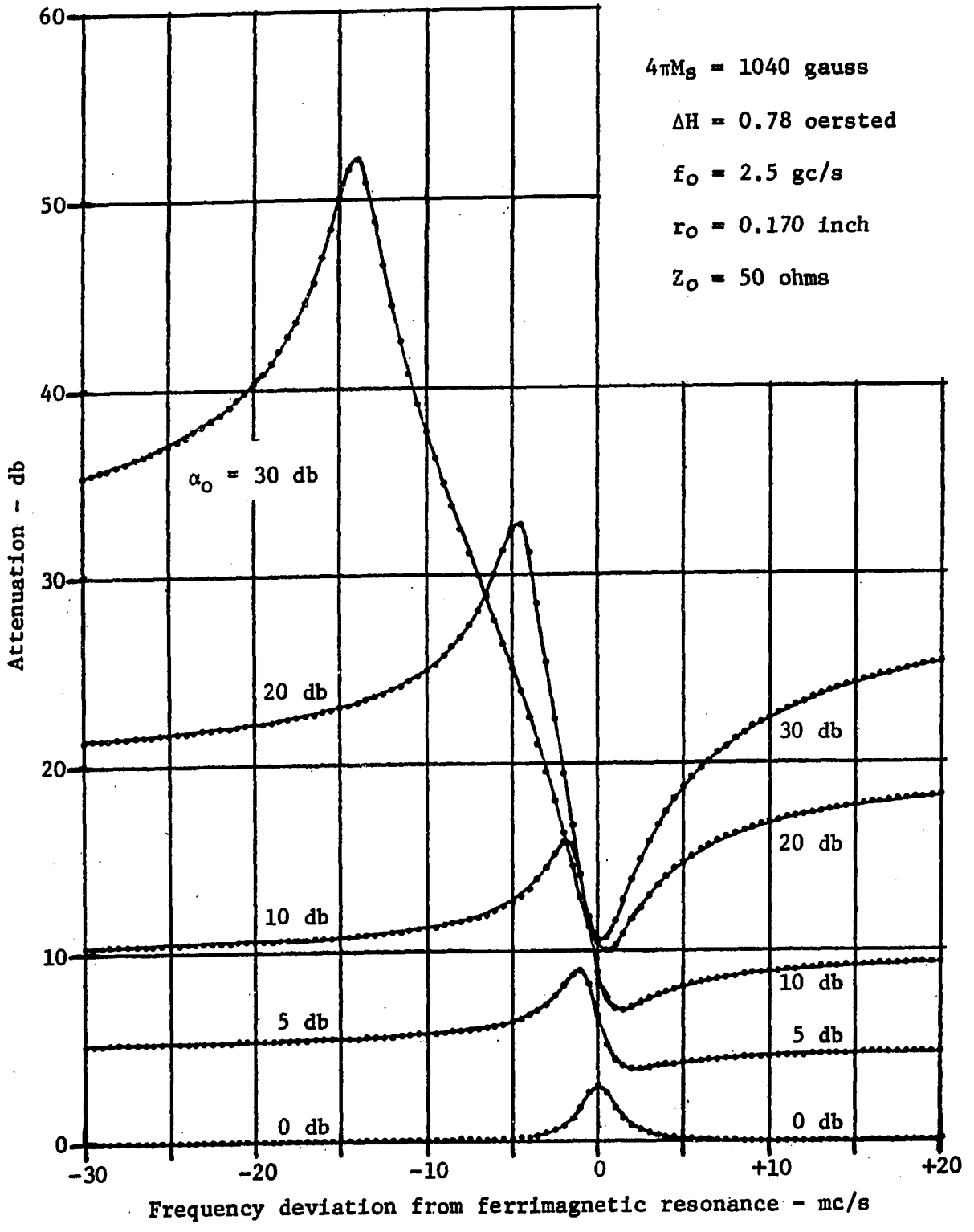

Figure 15. Computer solutions to Equation 61 with line width twice that of Figure 12

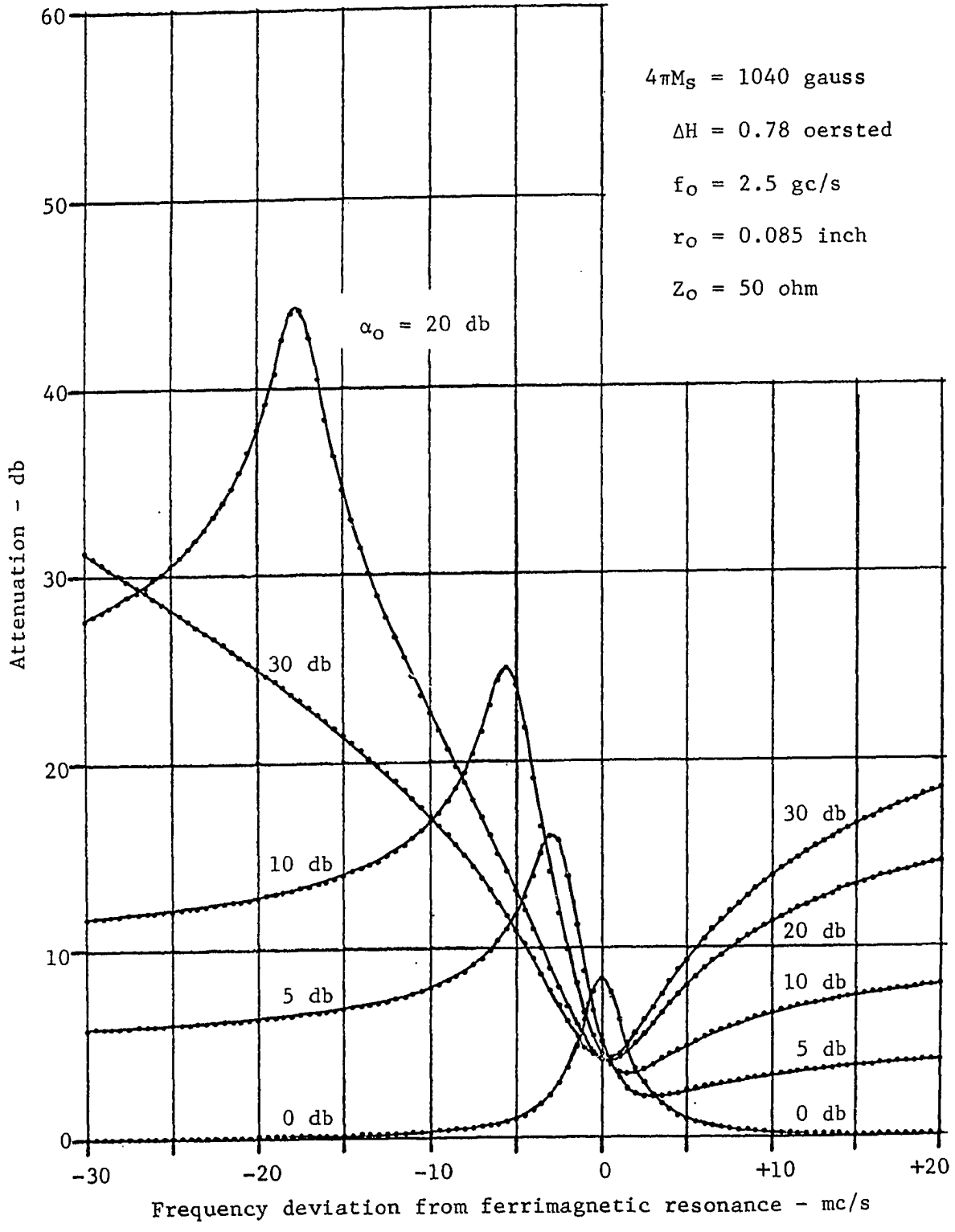

Figure 16. Computer solutions to Equation 61 with line width twice that of Figure 13

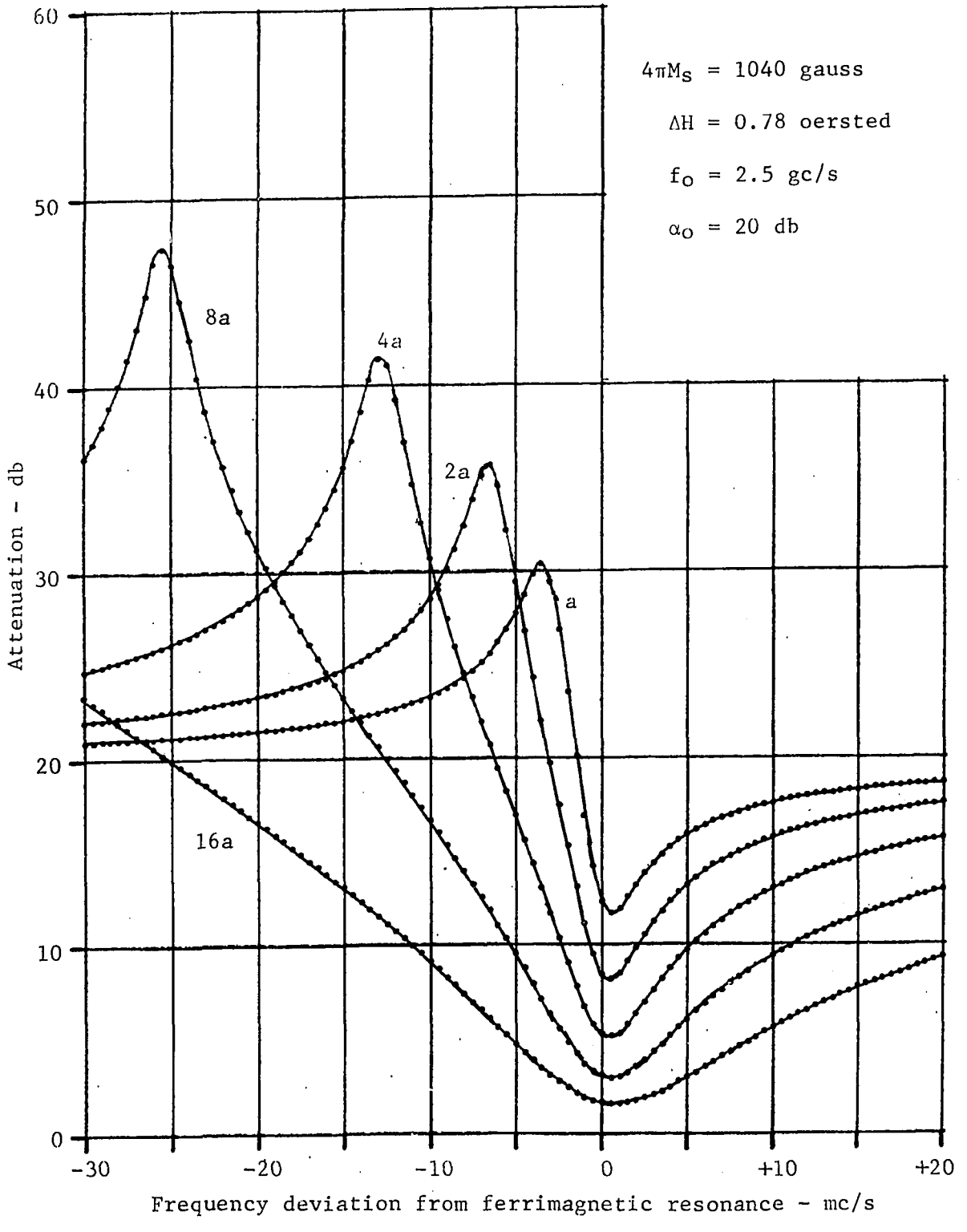

Figure 17. Computer solutions to Equation 61 for various values of the coupling parameter a and wider line width

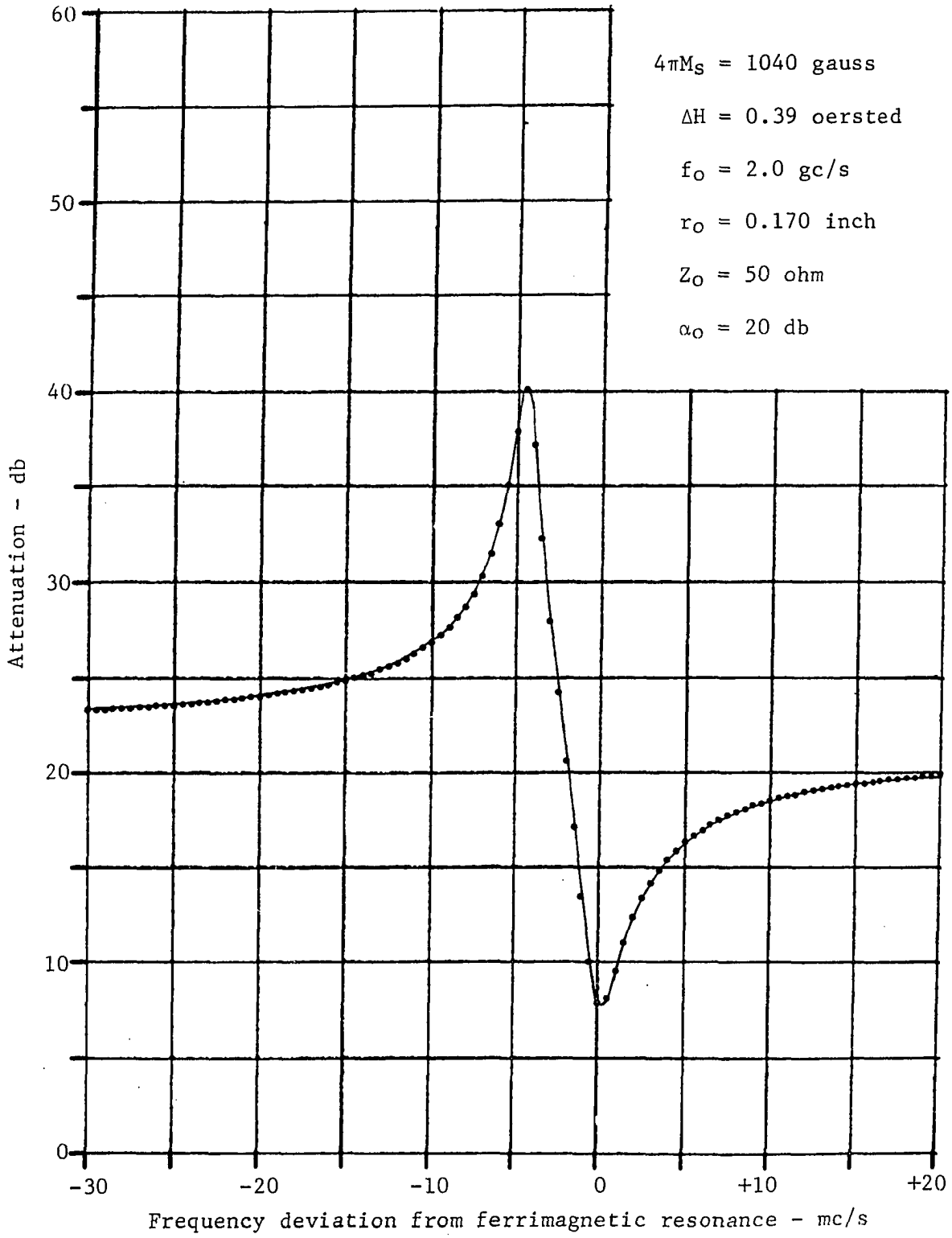

Figure 18. Computer solutions to Equation 61 with ferrimagnetic resonance frequency at 2.0 gc/s

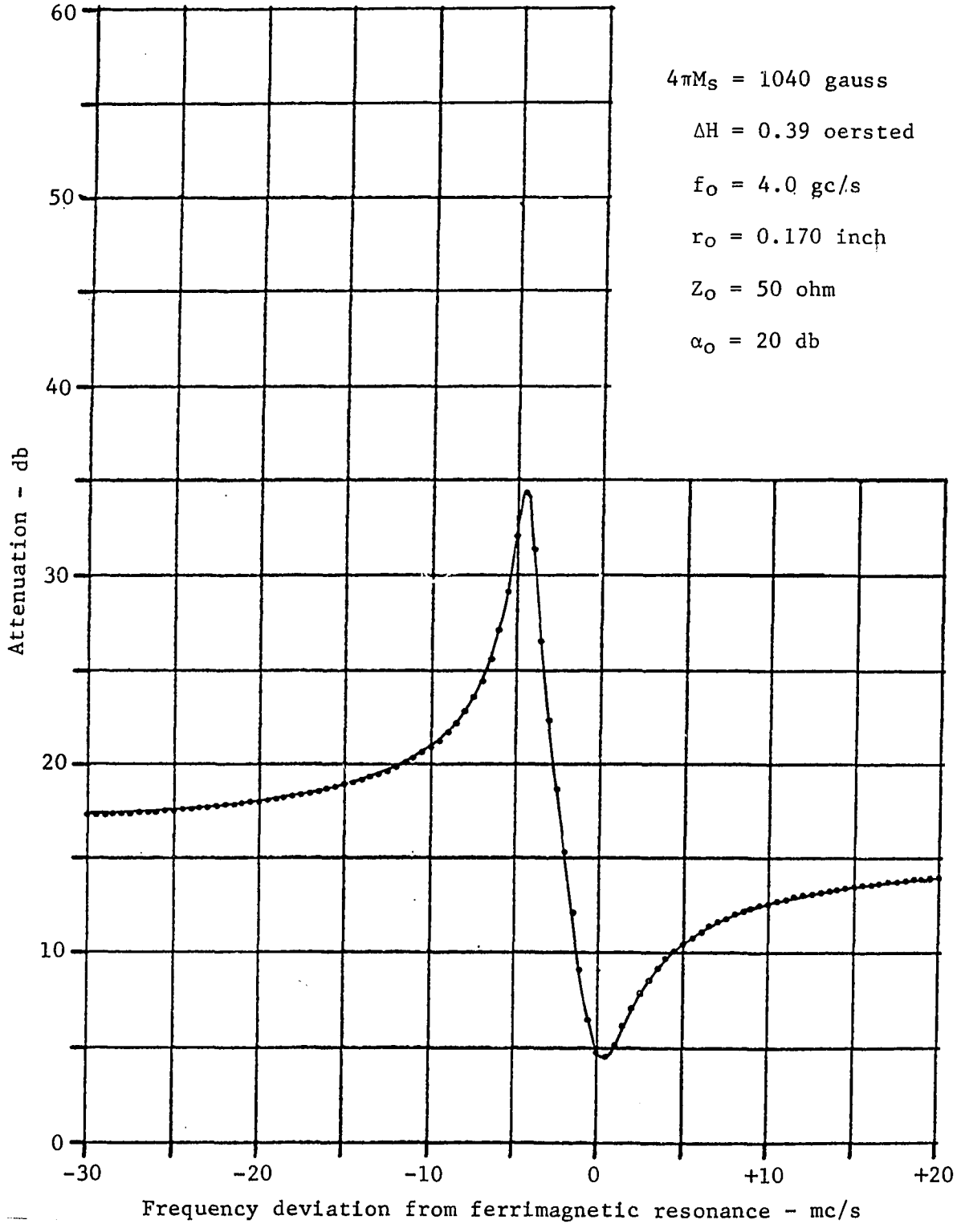

Figure 19. Computer solutions to Equation 61 with ferrimagnetic resonance frequency at 4.0 gc/s

2.5 gc/s has been plotted for several values of aperture attenuation α_o. The sphere was located at a radial distance $r_o = 0.170$ inch and the line width, which appears implicitly in a, was 0.39 oersted. For the band reject case, which corresponds to $\alpha_o = 0$, the attenuation at ferrimagnetic resonance was 5.18 db. For all cases in which an iris provides an initial attenuation $\alpha_o \neq 0$, the response displays a "discriminator" characteristic. Attenuation greater than the initial value would be classified as a band reject response, attenuation less than the initial value would be classified as a band pass response. Although the total response appears to be symmetrical about the attenuation of the iris, the logarithmic scale exaggerates the band reject portion of the curves.

In Figure 13, similar characteristics have been plotted for the sphere located at a radial distance $r_o = 0.085$ inch, which corresponds to an increase in the coupling between the magnetization of the sphere and the electromagnetic fields in the transmission line. The higher coupling causes higher peak attenuation for the band reject case and lower insertion loss for the band pass situations.

Since coupling between the magnetization of the sphere and the fields of the line manifests itself in the analytical parameter a, the attenuation versus frequency deviation characteristics have also been plotted for a fixed value of α_o and several values of a.

In practice the ferrimagnetic sphere will be located in close proximity to conducting walls; therefore, degradation of the unloaded Q of the resonator is unavoidable. To determine the effects of a lower Q_u, the computations presented in Figures 12, 13 and 14 were repeated

with $\Delta H = 0.78$ oersted or twice its original value. These data are presented in Figures 15, 16 and 17, respectively. As expected, the response curves are broader than before and the maximum and minimum attenuations do not deviate as far from the initial values of attenuation. An examination of the figures will also show that a lower Q_u reduces the differences between minimum and maximum attenuations of the response curves in the same manner as a smaller value of a. However, a lower Q_u broadens the response curves much more than a reduction in coupling.

Figures 18 and 19 demonstrate the effect of the ferrimagnetic resonance frequency upon the response behavior. In Figure 18 the resonance frequency was 2 gc/s and in Figure 19 it was 4 gc/s. In both cases, $\alpha_o = 20$ db. The response curves maintain their general shape, but coupling effectively increases with increased frequency.

C. Development of Mathematical Model for YIG Sphere in Aperture of Coaxial Iris Discontinuity

The equivalent circuit for a YIG resonator mounted in an orthogonal coupling structure has been developed by Carter (6) and others (7). Comstock (39) developed an equivalent circuit for a YIG resonator in a band reject application. None of these equivalent circuits adequately describe the YIG resonator and coupling structure which includes an iris discontinuity in the transmission line. To develop the mathematical model for the coaxial structure described herein, we postulate the circuit of Figure 20 to represent the system near ferrimagnetic resonance. The series RLC circuit represents the ferrimagnetic resonator, the inductive reactance X_o represents the iris discontinuity in the transmission line

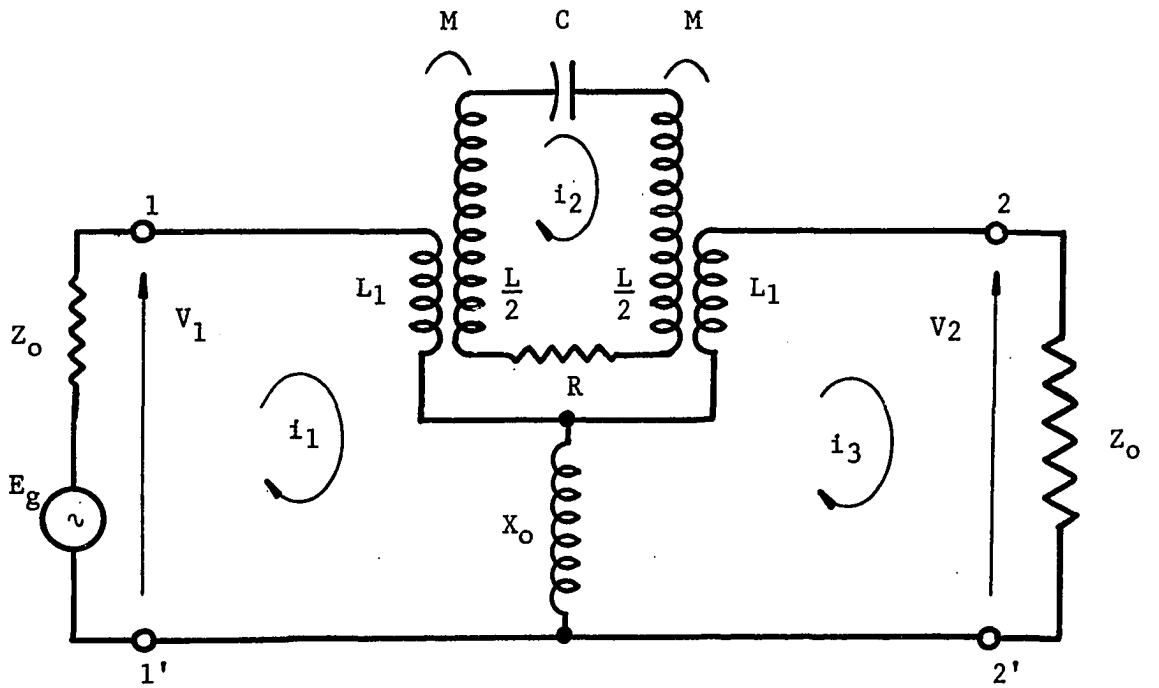

Figure 20. Equivalent circuit postulated for YIG sphere mounted in coaxial coupling structure with iris discontinuity

and the identical transformers located on each side of the iris reactance represent the symmetrical coupling to the input and output transmission lines (YIG centered in the aperture).

Qualitatively, the circuit satisfies the two extremes of coupling for the physical system. First, if there is no iris discontinuity in the transmission line, the structure behaves as a band reject filter. In this case X_o is infinite and the circuit indeed reduces to the equivalent circuit of a band reject filter. Second, if the aperture in the iris discontinuity is extremely small, coupling between the input and output transmission lines can only be accomplished through the YIG resonator. In this case X_o is essentially zero and coupling exists only through the mutual inductance of the resonator circuit. A quantitative description can be made by determining the transmission coefficient of the equivalent circuit and comparing it term by term with the transmission coefficient previously obtained by means of the field analysis.

For the circuit of Figure 20, the voltage transmission coefficient equivalent may be defined as

$$T(j\omega) = \frac{V_2}{V_1} = \frac{2\ Z_o i_3}{E_g} . \tag{65}$$

The output voltage is referred to the voltage at the terminal 1-1' rather than the voltage at the generator to be consistent with the previous field analysis in which the output was referred to the incident field.

The loop current equations for the circuit,

$$[Z_o + jX_o + j\omega(L_1 + M)]\ i_1 - j\omega M\ i_2 - jX_o i_3 = E_g \tag{66}$$

$$- j\omega M\, i_1 + [R + j\omega L + j2\omega M - j/\omega C]\, i_2 - j\omega M\, i_3 = 0 \qquad (67)$$

$$- jX_o i_1 - j\omega M\, i_2 + [Z_o + jX_o + j\omega(L_1 + M)]\, i_3 = 0, \qquad (68)$$

can be simplified by making the following assumptions based on the fact that the resonator has a very high unloaded Q:

$$X_o >> \omega L_1,\ X_o >> \omega M,\ L >> M,\ \omega_o = (1/LC)^{1/2} . \qquad (69)$$

The circuit determinant Δ then becomes

$$\Delta = \begin{vmatrix} Z_o + jX_o & - j\omega M & - jX_o \\ - j\omega M & R + jL(\omega^2 - \omega_o{}^2)/\omega & - j\omega M \\ - jX_o & - j\omega M & Z_o + jX_o \end{vmatrix} , \qquad (70)$$

which can be solved to obtain

$$\Delta = (Z_o + j2X_o)\,[Z_o R + 2\omega^2 M^2 + j\, Z_o L\, (\omega^2 - \omega_o{}^2)/\omega]. \qquad (71)$$

The current i_3 is obtained by the expression

$$i_3 = \frac{\begin{vmatrix} Z_o + jX_o & - j\omega M & E_g \\ - j\omega M & R + jL(\omega^2 - \omega_o{}^2)/\omega & 0 \\ - jX_o & - j\omega M & 0 \end{vmatrix}}{\Delta}$$

which yields

$$\frac{i_3}{E_g} = \frac{-\omega^2 M^2 + jX_o[R + jL(\omega^2 - \omega_o{}^2)/\omega]}{(Z_o + j2X_o)[Z_o R + 2\omega^2 M^2 + jZ_o L(\omega^2 - \omega_o{}^2)/\omega]} . \qquad (72)$$

Therefore, the transmission coefficient for the circuit of Figure 20 becomes

$$T(j\omega) = \frac{2Z_o\{-\omega^2 M^2 + jX_o[R + jL(\omega^2 - \omega_o{}^2)/\omega]\}}{(Z_o + j2X_o)[Z_o R + 2\omega^2 M^2 + jZ_o L(\omega^2 - \omega_o{}^2)/\omega]} . \qquad (73)$$

To compare Equation 73 with Equation 60, the expression obtained by the field analysis, it is necessary to multiply numerator and denominator by $j\frac{\omega}{Z_o L}$; thus

$$T(j\omega) = \frac{2\{-\omega X_o R/L + j[X_o(\omega_o^2 - \omega^2) - \omega^3 M^2/L]\}}{(Z_o + j2X_o)[\omega_o^2 - \omega^2 + j\omega(R + 2\omega^2 M^2/Z_o)/L]} \quad . \quad (74)$$

If

$$2\omega_o \alpha = R/L, \quad (75)$$

and

$$Z_o a \omega_o \omega_m = 2\omega^2 M^2/L \quad , \quad (76)$$

then Equation 74 is equivalent to Equation 60.

We can examine the conditions imposed by Equations 75 and 76 in other forms. Substituting for α and inverting, Equation 75 becomes

$$Q_u = \omega_o L/R, \quad (77)$$

which clearly emphasizes the equivalence between the ferrimagnetic resonator and a lumped parameter circuit. Substituting for a, Equation 76 becomes

$$\frac{\mu_o v_f \omega_o \omega_m}{2\pi^2 r_o^2} = \frac{2\omega^2 M^2}{L} \quad . \quad (78)$$

The equivalence is not so obvious in this expression, but the fact that the self inductance and mutual coupling are functions of geometrical factors only indicates a striking similarity.

IV. EXPERIMENTAL FINDINGS

To experimentally verify some of the analytical results obtained for the coaxial coupling structure with a single resonator, the assembly sketched in Figure 7 was constructed. The diameters of the brass coaxial conductors were made identical to those of standard General Radio test accessories so that GR Type 874 fittings could be used to attach external cables. Irises for controlling the coupling where chemically etched from 0.003-inch thick sheets of beryllium-copper. Screw-type fittings for the inner and outer conductors were employed to clamp the edges of the iris so that leakage would be kept to a minimum. The dielectric support was a 1/4-inch thick doughnut made from a Rexolite[3] rod. Photographs of the completed coaxial assembly and its component parts are shown in Figures 21 and 22.

Samples of Ga-YIG spheres were purchased from Airtron, Morris Plains, New Jersey. The saturation magnetizations and line widths of the spheres were measured by Airtron and the data furnished with the samples. Table 2 lists the characteristics of the three spheres available. Each sphere was mounted on the tip of a 2-56 nylon screw by means of an epoxy adhesive. One of the easy axes of magnetization was aligned parallel with the axis of the screw by placing the sphere in the field of a strong electromagnet. In this operation the axis of the screw was placed parallel to the field and the strength of the magnetic field required to cause alignment was determined by using a microscope to observe the motion

---

[3]Registered trademark

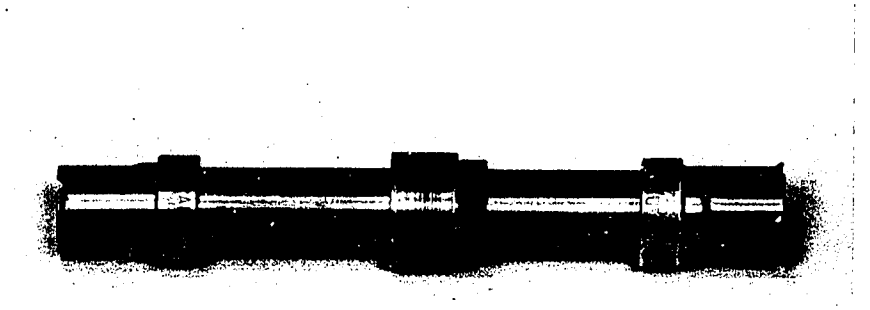

Figure 21. Assembled coaxial structure for Ga-YIG filter with aperture coupling

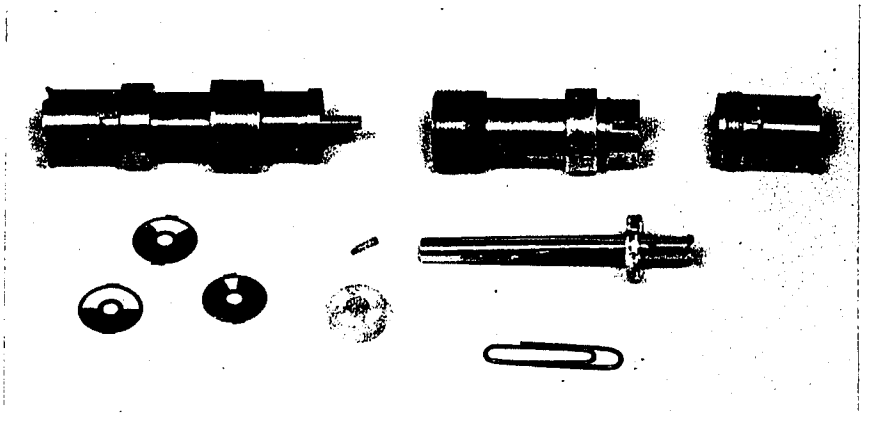

Figure 22. Disassembled coaxial structure with several apertures; r_o = 0.170 inch

Table 2. Ferrimagnetic properties of Ga-YIG spheres used to obtain experimental data

Serial Number	Diameter d (inches)	Saturation Magnetization M (gauss)	Line Width ΔH (oersteds)	Q_u at 2.5 gc/s
4Ga-8	0.051	1040	0.39	2290
17Ga-5	0.0502	985	0.45	1985
17Ga-8	0.0504	985	0.45	1985

of the Ga-YIG sphere.

Magnetic bias for the experiments was supplied by a solenoidal electromagnet placed around the coaxial structure. The solenoid was designed to provide a large region of uniform field intensity without regard for efficiency. Power for the electromagnet was obtained from a 0-10 ampere current-regulated Harrison Labs 809A power source. Regulation of the power supply was rated at 10 milliamperes, ripple at 5 milliamperes.

Experimental measurements were made over a range of frequencies about 2.5 gc/s. A block diagram of the test apparatus used to measure the attenuation α_r is shown in Figure 23. Considerable difficulty was experienced in obtaining accurate quantitative data due to instrumentation limitations. However, qualitative verification of the analytical results was obtained with relative ease.

Referring to the block diagram, a Hewlett Packard Model 616B, which covers the 1.8 to 4.2 gc/s frequency range and has a maximum power output

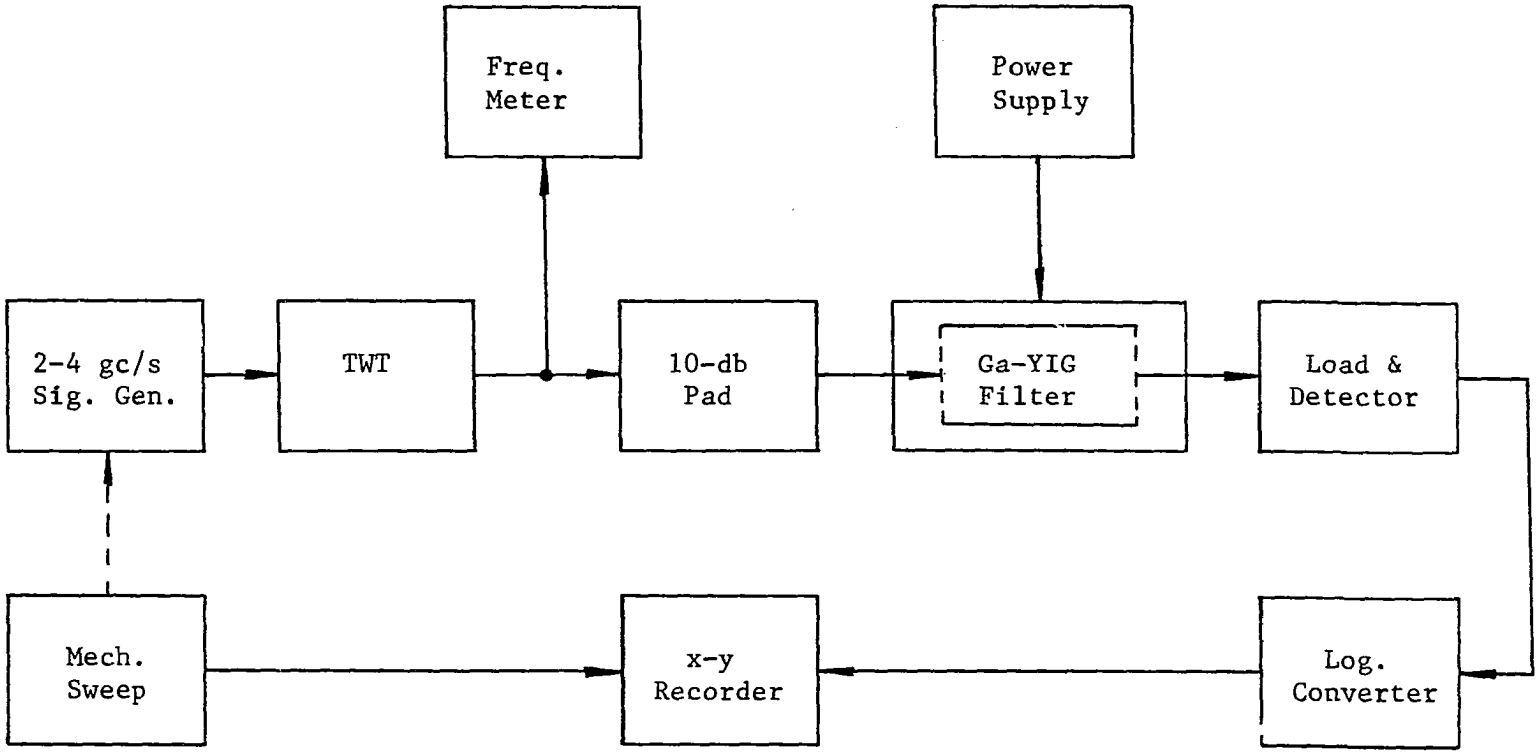

Figure 23. Block diagram of test apparatus

of about one milliwatt (mw), was fed into a Hewlett Packard Model 491C traveling-wave-tube (TWT) microwave amplifier which has a maximum gain of about 30 db. To avoid saturating the amplifier, the gain of the TWT was reduced so that the TWT output was only 100 mw. A 10-db attenuator was attached to the output of the TWT as a precaution to prevent reflections from the ferrimagnetic resonator filter from disturbing the signal source. The final 10-mw signal was then applied to the experimental filter. The frequency of the signal was measured by an F-R Machine Works Type N410A frequency meter.

To measure the filter characteristics, a Hewlett Packard Model 423A microwave load and detector was connected to the output of the filter. The dc voltage from the detector was fed to a Moseley Model 60 DM logarithmic converter which changed the linear output of the detector to a decibel equivalent. The output of the logarithmic converter was then fed to the y-axis input of a Moseley Model 2, two-axis recorder. A General Radio Type 1750-A mechanical sweep mechanism was used to sweep the frequency of the signal generator and also provide a sweep voltage for the x-axis input of the x-y recorder. By scaling the y-axis of the recorder in decibels and the x-axis in mc/s, it was possible to obtain a graphical display of the response through the ferrimagnetic resonator filter.

Precise measurements of the response characteristics were not possible due to several reasons: (1) Power supply drift, (2) residual amplitude and frequency modulation appearing on the signal source, (3) very low frequency response of the logarithmic converter and x-y recorder, and (4) numerous mechanical instabilities. However, the response shapes were

repeatable; maximum and minimum attenuations were within ± 1 db for most tests. Experimental errors and deviations from calculated values were greatest for the measurements performed with high values of intial attenuation.

Figures 24 through 27 are reproductions of the experimental response characteristics obtained using sphere serial number 4Ga-8 mounted at the radial distance $r_o = 0.170$ inch. These four curves correspond to $\alpha_o = 0$ db, 5 db, 10 db and 20 db. The peak variations in attenuation, α_{max} and α_{min}, are compared with their analytical counterparts from Figures 12 and 15 in Table 3.

Table 3. Comparison of calculated and experimental peak values of attenuation for $r_o = 0.170$ inch (all values in db)

Initial attenuation		Calculated, Q_u		Experimental		Calculated, $Q_u/2$	
Calc. α_o	Exp. α_o	α_{max}	α_{min}	α_{max}	α_{min}	α_{max}	α_{min}
0	0	5.2	-	4.9	-	3.0	-
5	5.1	12.0	3.1	11.5	3.2	9.1	3.9
10	10.0	20.0	5.2	18.8	6.0	16.0	7.0
20	20.2	38.4	6.7	27.3	10.2	32.8	10.1
	22.4			30.0	10.7		
30		58.2	7.0	36.0	12.4	52.2	10.7

In practice, α_{min} from Table 3 would correspond to insertion loss for the band pass filter. For α_o less than 20 db, all measured values

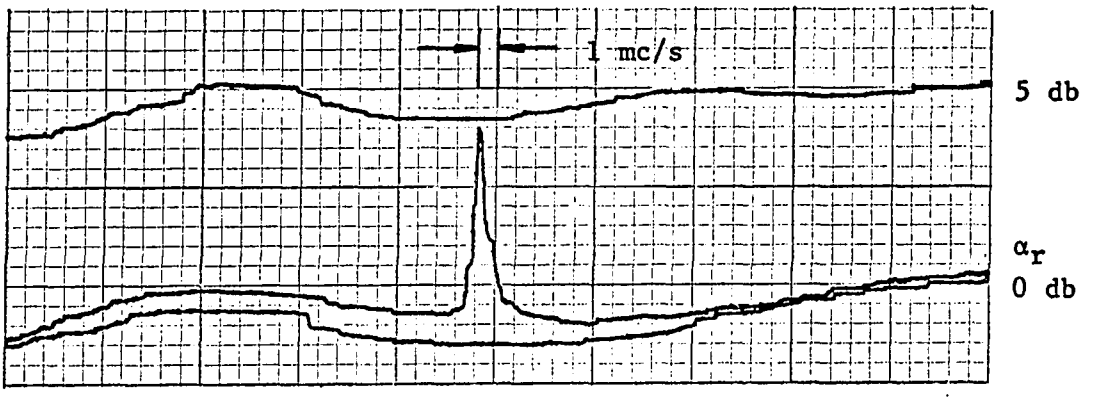

Figure 24. Experimental filter characteristics for r_o = 0.170 inch and α_o = 0 db

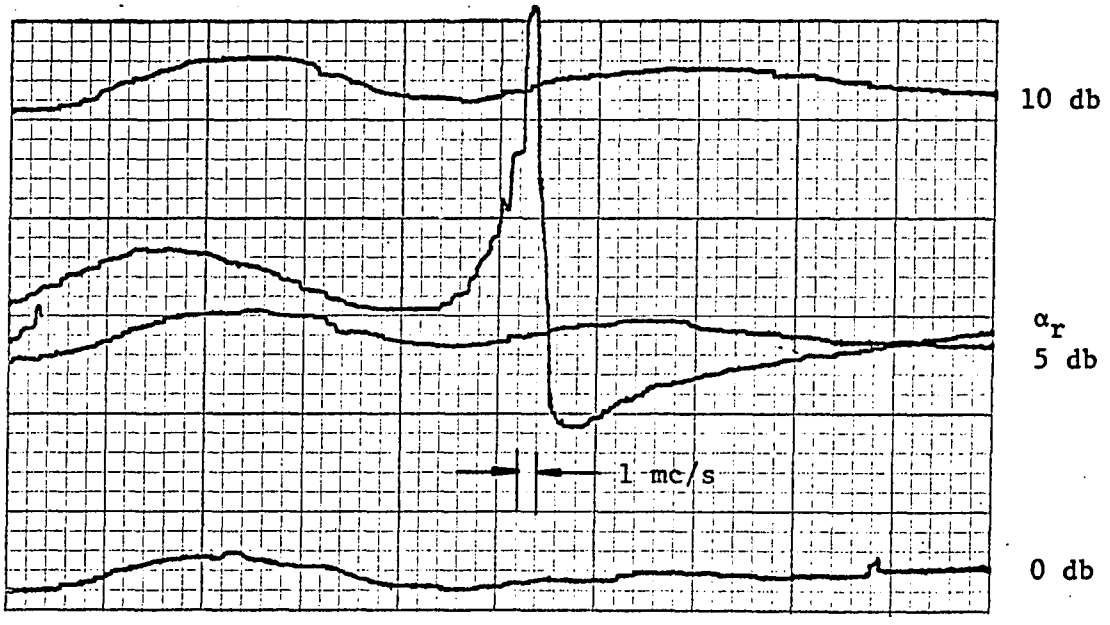

Figure 25. Experimental filter characteristics for r_o = 0.170 inch and $\alpha_o \approx$ 5 db

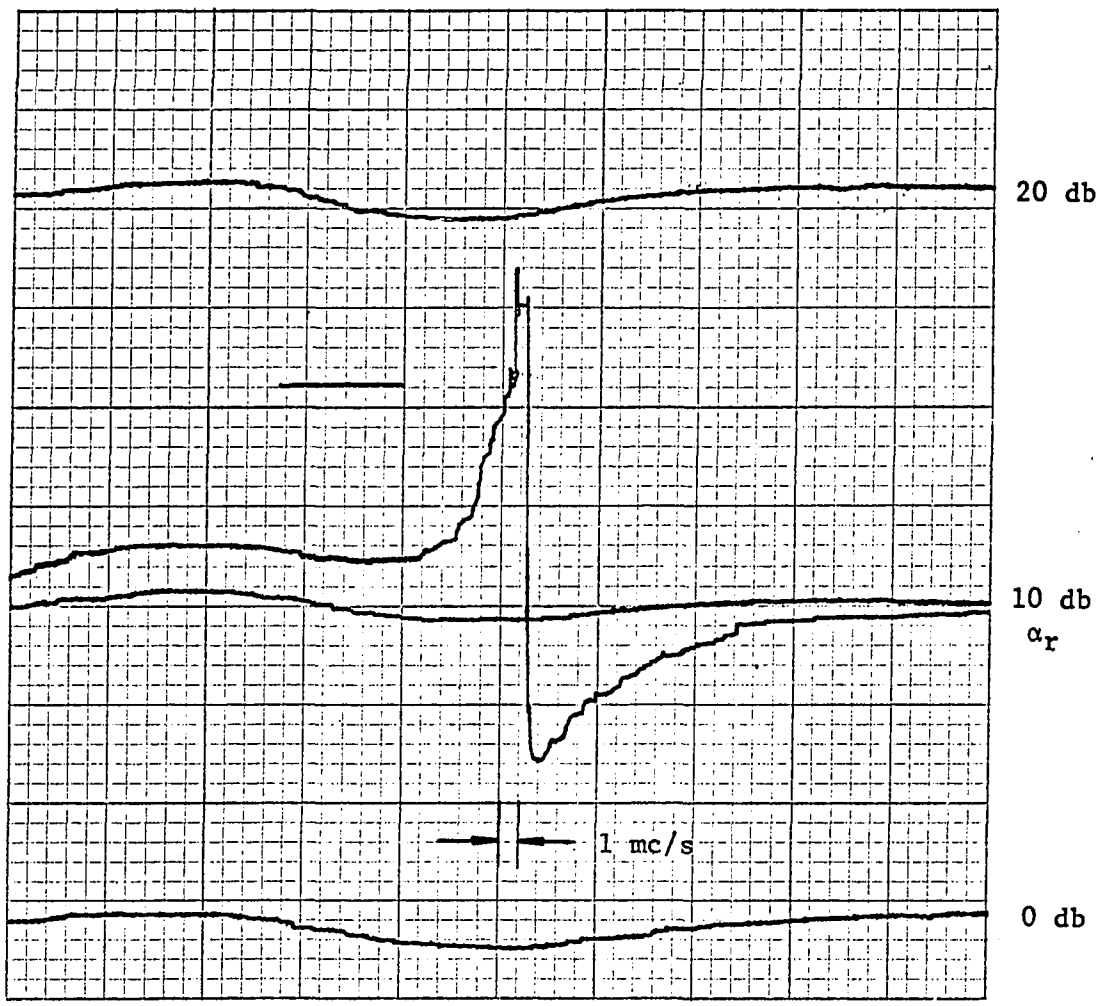

Figure 26. Experimental filter characteristics for r_o = 0.170 inch and α_o = 10 db

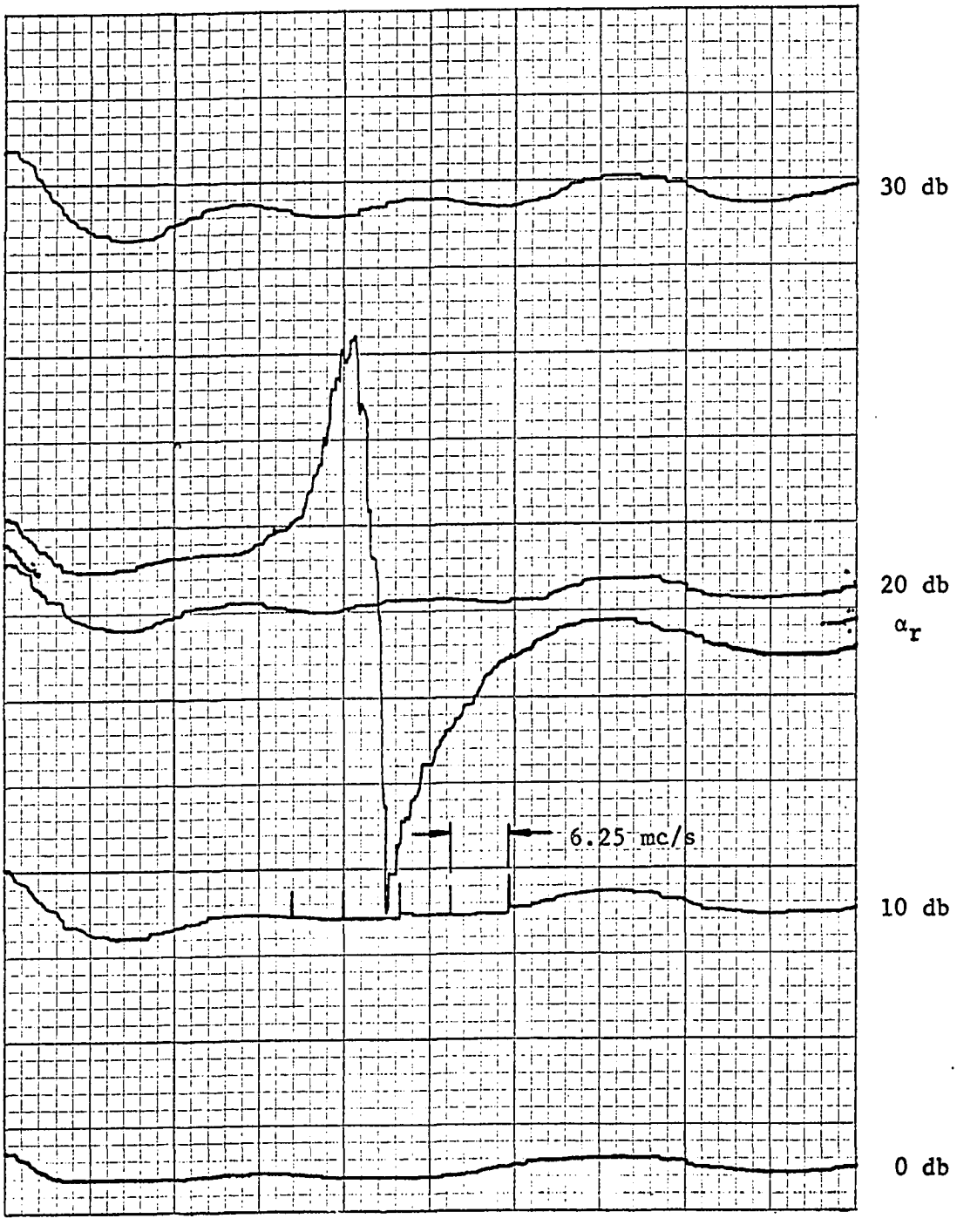

Figure 27. Experimental filter characteristics for r_o = 0.170 inch and $\alpha_o \approx$ 20 db

of α_{min} were between the two calculated values determined by Q_u and $Q_u/2$. The frequency differences between two points of equal attenuation on the experimental responses were, in general, wider than the corresponding differences on the analytical plots of Figure 12. Since the sphere was within 0.023 inch of the center conductor, it is reasonable that the proximity of the transmission line caused degradation of the resonator. However, one should not overlook the fact that less coupling will affect the amplitude of α_{min} in much the same way.

In practice, α_{max} from Table 3 would correspond to a band reject filter. For values of initial attenuation less than 20 db, the values of α_{max} were also between the two calculated values. This result is consistent with the conclusion that the unloaded Q had been degraded. For initial attenuations of 20 db and 30 db the measured values of α_{max} appear to be well behaved, but they differ considerably from the calculated values. This indicates that the field analysis does not adequately predict the behavior of the α_{max} for large values of initial attenuation. Since this situation is of little practical interest, it was not pursued further in this investigation.

To demonstrate the effect of tighter coupling, a second coaxial structure with reduced dimensions was constructed so that the sphere could be mounted at $r_o = 0.085$ inch. The complete assembly and its component parts are shown in Figure 28. The center conductor was tapered to a diameter of 0.098 inch and the inner surface of the outer conductor was also tapered to maintain a 50-ohm characteristic impedance. As before, irises were chemically etched from 0.003-inch thick beryllium-copper sheets.

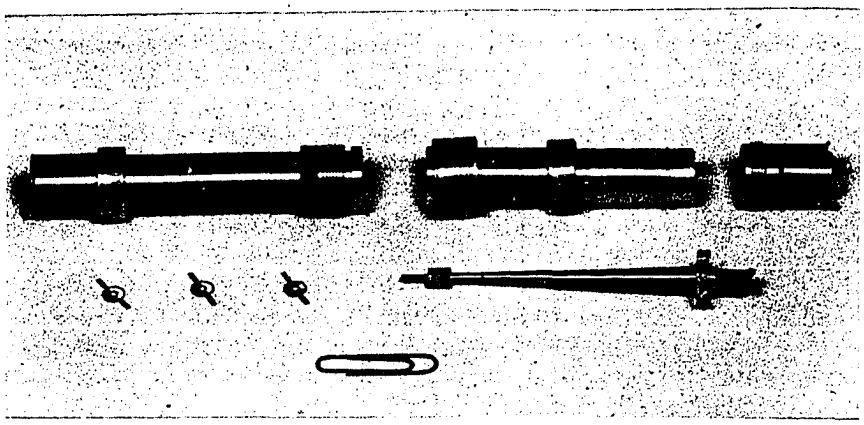

Figure 28. Disassembled coaxial structure with taper to increase coupling; r_o = 0.085 inch

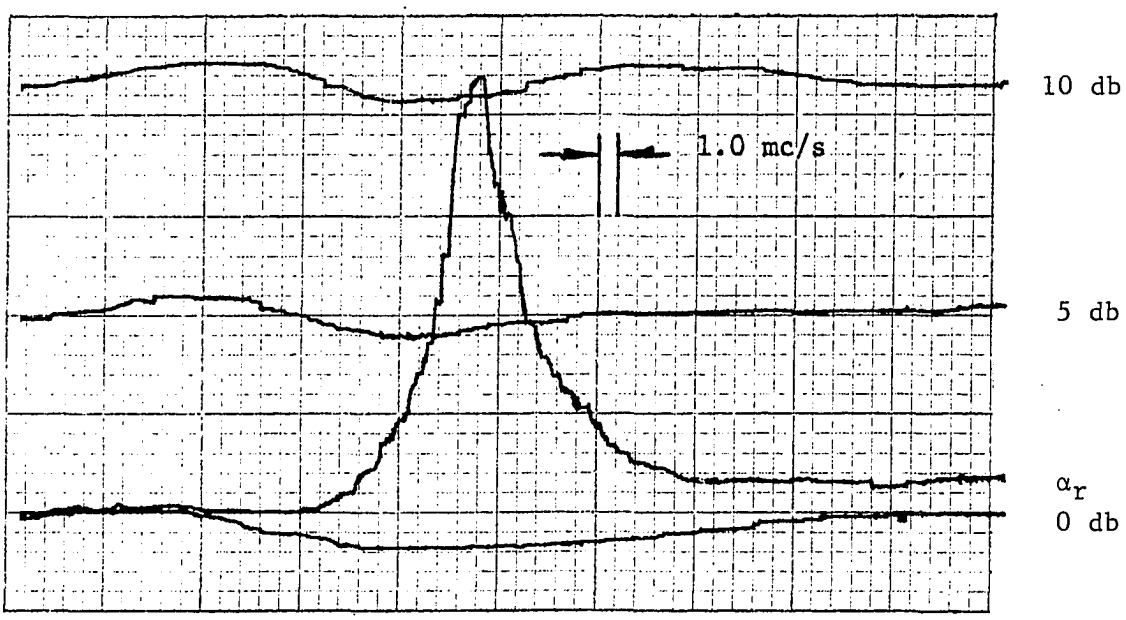

Figure 29. Experimental filter characteristics for r_o = 0.085 inch and without iris

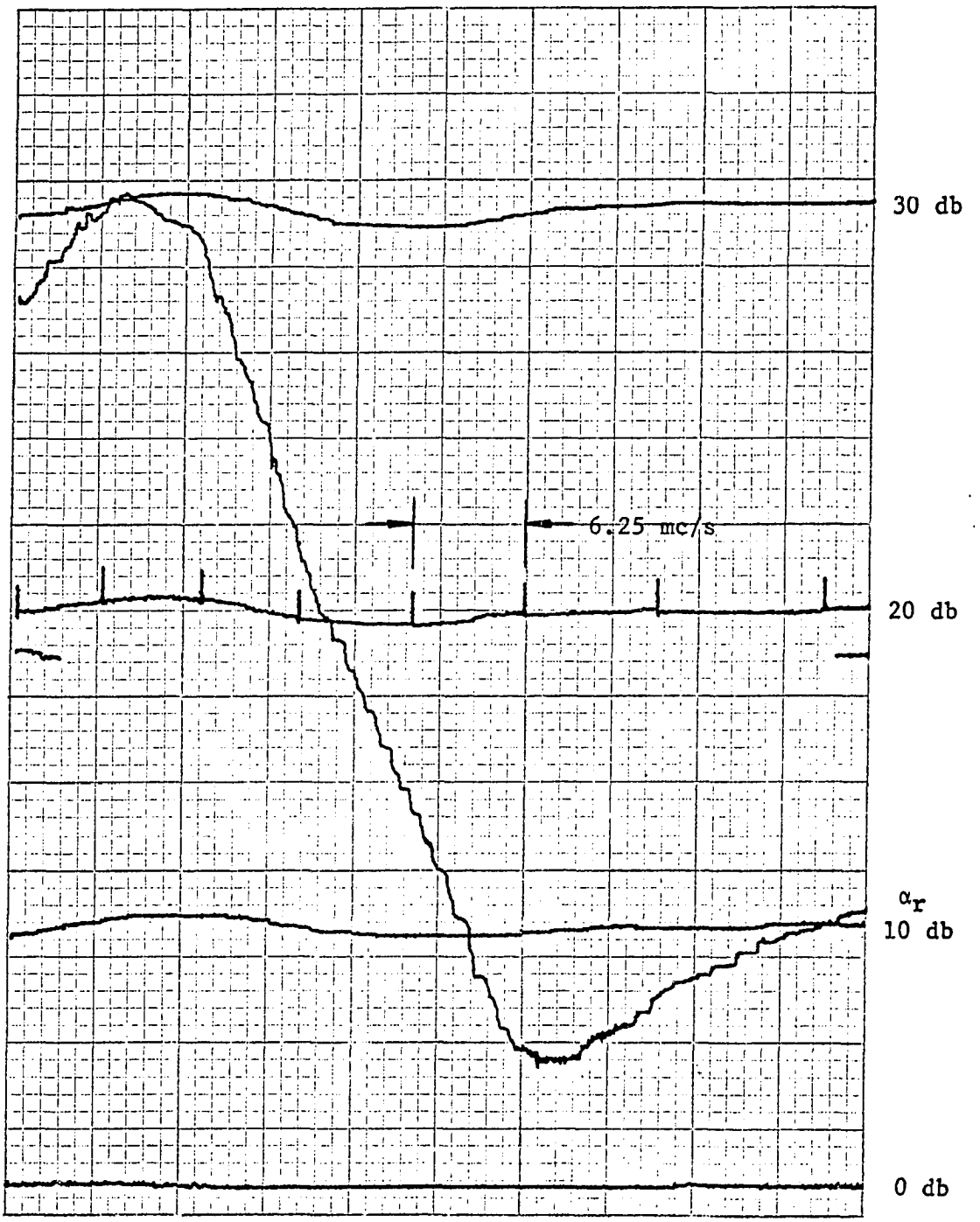

Figure 30. Experimental filter characteristics for r_o = 0.085 inch and $\alpha_o \simeq$ 20 db

Figures 29 and 30 are reproductions of the experimental response characteristics for α_o = 0 db and 20 db and r_o = 0.085 inch. These curves are compared to their respective analytical curves presented in Figures 13 and 16. As expected the maximum attenuation for the band reject filter (see Figure 29) increased as a result of tighter coupling, but the value of 10.9 db differed from the predicted value of 12.6 db by a greater margin than that of the previously described structure when r_o = 0.170 inch. This result is reasonable. Since the sphere was located less than 0.010 inch from both the inner and outer conductors, a much lower Q_u than before could be expected. A second factor must also be considered and that is the assumption that the resonator was located in a uniform magnetic field. In this structure, the dimensions of the line were reduced considerably while the diameter of the sphere remained fixed. Therefore, the field of the TEM mode could not be uniform throughout the volume of sphere. The experimental results indicate that the consequences of a non-uniform field are not severe, but the need for tighter coupling in practice may make stripline structures more attractive for band reject applications.

The reduced Q_u of the resonator is very apparent in the response characteristic of Figure 30, where α_o was 18.6 db, α_{max} was 30.1 db, α_{min} was 5.2 db and the frequency difference between these two attenuations was 27 mc/s. (Each vertical mark on the 20-db line represents 6.25 mc/s.) The value of α_{min} indicates an unloaded Q less than either of the values used for calculations. Nevertheless, the value of α_{min} was lower than the corresponding value obtained for r_o = 0.170 inch

which verifies that coupling can be increased by reducing the radial position of the sphere.

Since previous investigators have used coupling structures featuring orthogonal coupling of the input and output fields within the resonator, a similar structure was assembled using coaxial elements. The assembled structure and its component parts are shown in Figures 31 and 32. The coupling aperture was located in an iris at the common ends of the input and output coaxial transmission lines. The axes of the lines were displaced so that the radius vector of one line was perpendicular to the radius vector of the other line at the center of the aperture. A brass block supported the two sections of line and the iris. This structure approximates a structure with zero coupling in the absence of a resonator. However, the field analysis and transmission equations developed previously are no longer applicable because the electromagnetic fields do not couple to the magnetic moment of the resonator in the same manner. In the orthogonal structure the fields of the input line couple to the x component of magnetization, while the fields of the output line couple to the y component of magnetization. In the analysis for this study the fields of both the input and output lines were coupled to the x component.

The experimental response curve of the orthogonally coupled structure is shown in Figure 33. As expected, only a band pass characteristic was observed because the initial attenuation was beyond the capabilities of the measurement set-up. The effective bandwidth of the filter was wider than for the structures investigated previously, but the

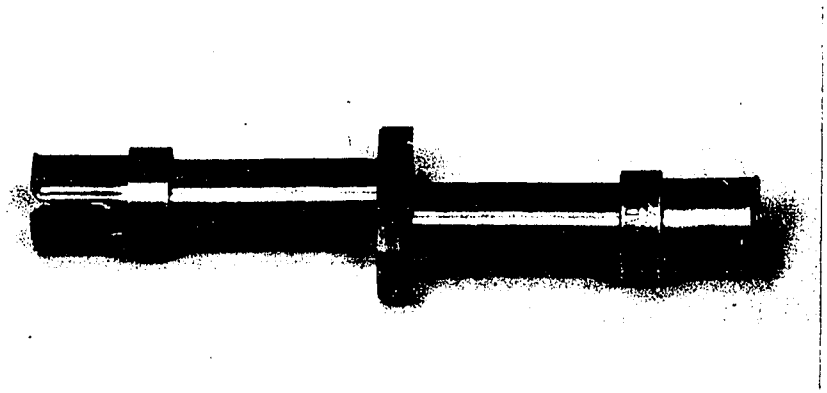

Figure 31. Assembled coaxial structure for Ga-YIG filter with orthogonal aperture coupling

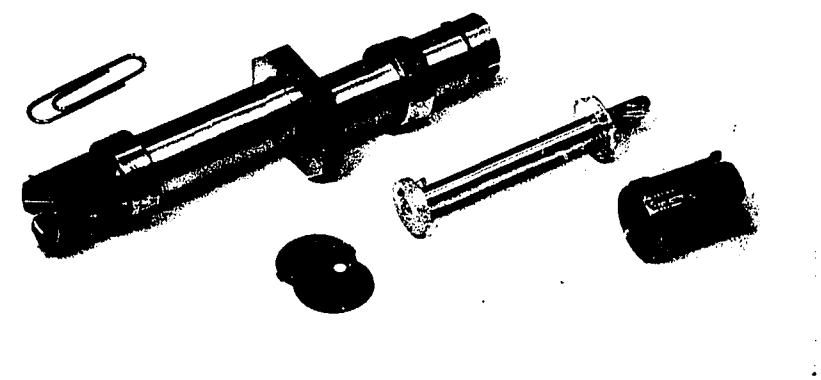

Figure 32. Disassembled coaxial structure and aperture for orthogonal coupling; r_o = 0.170 inch

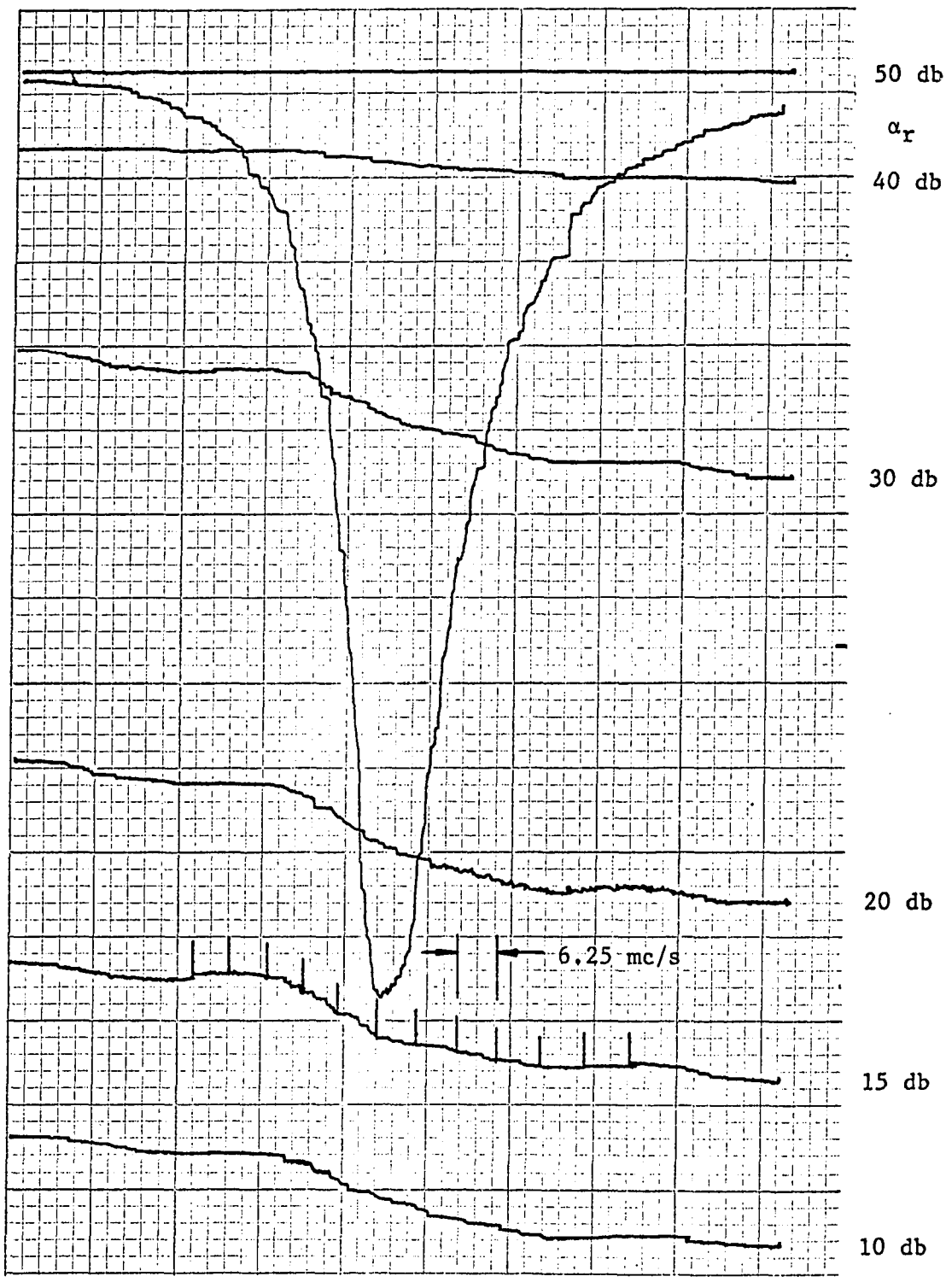

Figure 33. Experimental filter characteristics for orthogonally coupled structure; r_o = 0.170 inch

insertion loss was also an impractical 15 db whereas a useful value would be much lower. The radial position of the sphere was $r_o = 0.170$ inch, therefore, the insertion loss could be improved by tighter coupling. In practice, the displaced axes of this structure create a problem for the design of a dc magnetic bias which may be difficult to overcome.

For all measurements with small apertures, the position of the sphere was found to be important in obtaining best performance. For a 90° aperture and $r_o = 0.170$ inch, α_{min} for the structure of Figure 7 would increase 2 to 3 db when the sphere was placed close to the edge of the aperture. This increase in attenuation was probably due to higher induced currents in the conducting iris causing an increase in the losses within the Ga-YIG material. When the sphere was withdrawn from the aperture about 0.025 inch along the axis of the line, the minimum attenuation increased about 2 db. Theoretically, there should have been no coupling to the output line in this case. Therefore, these results indicate that there is some fringing of the fields through the aperture. For large apertures, the effects were less significant.

The axial position of the sphere was extremely critical for the orthogonal structure. The aperture was a 0.125-inch diameter circle and the insertion loss would change 10 to 15 db for a movement of about 0.010 inch in the axial position.

In all of the above measurements, the responses were essentially symmetrical when the source and load were interchanged. Similarly, the magnitudes of the responses were not affected by reversing the polarity of the dc magnetic bias on the filter.

As a final qualitative experiment, the remaining two resonators listed in Table 2 were mounted on opposite sides of the plane of the iris of the first coaxial structure investigated. Typical two-resonator band pass filter responses ranging from under-coupling to over-coupling could be obtained by varying the axial position of the two spheres, thus suggesting an area for future investigation.

V. CONCLUSIONS

The investigation reported in the preceeding pages was concerned with determining the response characteristics of a magnetically biased ferrimagnetic resonator located in the aperture of an iris in a coaxial transmission line. The problem was solved analytically by determining the reflection and transmission coefficients of the system. In the analysis the resonator was assumed to be magnetically saturated along the direction of the axis of the transmission line and the microwave field was assumed to consist of only the TEM mode and to be uniform throughout the volume of the sphere. Numerical results were obtained for various values of initial iris attenuation, coupling and ferrimagnetic resonance frequency. These results showed that a band pass and band reject characteristic could be obtained and that the attenuation, when plotted on a logarithmic scale as a function of the frequency deviation away from the ferrimagnetic resonance frequency, followed a discriminator-shaped curve which was essentially symmetric about the initial iris attenuation.

A mathematical model and equivalent circuit of the coaxial system was developed for the range of frequencies near the ferrimagnetic resonance frequency. The equivalent circuit consisted of an inductively coupled lumped parameter resonant circuit, which was analogous to the ferrimagnetic resonator, and a shunt inductance which was analogous to the iris discontinuity. For a large aperture, the shunt inductance would be very large and the equivalent circuit would behave as a band reject filter. For a very small aperture, the shunt inductance would also become small and the equivalent circuit would behave as a band pass filter. For

intermediate aperture sizes, the circuit would produce the "discriminator" characteristic.

Experimental efforts during this investigation verified all predicted results for small values of initial attenuation, although reduced Q_u was observed. For large values of initial attenuation, the differences between the experimental results and analytical predictions for maximum attenuation were significant. These differences were probably caused by the existence of higher-order modes within the sphere and/or line which were disregarded in the analytical approximations. The need to analyze these differences is not warranted by practical necessity.

The equivalence between the magnetically-biased ferrimagnetic resonator and a lumped parameter resonant circuit was established. Magnetic coupling between the resonator and the transmission line was shown to be a function of resonator position, saturation magnetization and volume, and the geometry of the transmission line. For a fixed coaxial geometry, coupling was increased by decreasing the radial position of the sphere or increasing the other sphere parameters. Conventional filter theory could be utilized to develop specified filter characteristics. Since the ferrimagnetic resonance frequency of the resonator was determined by an externally applied dc magnetic bias field, the response characteristics could be shifted to other microwave frequencies by electronic means in practice.

The high unloaded Q of single-crystal ferrimagnetic materials at microwave frequencies makes them particularly attractive for application in electronically-tuned band pass and band reject filters. The results of

this investigation suggest a number of possible applications and areas for future investigation.

One possible application is the use of the "discriminator" characteristic as the frequency detector for a feedback control loop to stabilize and sweep the frequency of a backward wave oscillator (BWO).

At the present state of the art most frequency discriminators at microwave frequencies are constructed using an array of transmission line phase shifting and coupling elements. Since the physical dimensions of the elements determine the frequency and phase characteristics, each discriminator must be designed for a particular application and is useful over a limited frequency range. The size is inversely proportional to the microwave frequency and may occupy several hundred cubic inches of volume. As frequency references for the purpose of stabilizing a BWO, transmission line discriminators are useful but they can not be rapidly swept over a range of frequencies. Therefore, they can not be used in new frequency scanning system applications.

Two electronically-tuned discriminators for scanning applications are just now being developed: The Pound discriminator and the two-resonator type that operates on the same principle as some low radio frequency discriminators. The Pound discriminator detects a wobbulated BWO signal that has been applied to a YIG filter. A feedback loop maximizes the second harmonic of the wobbulation frequency that is produced when the BWO frequency sweeps across the filter characteristic. Therefore, the feedback loop locks the BWO to the YIG resonance frequency. The other discriminator type utilizes two ferrimagnetic bandpass filters tuned to slightly

different resonance frequencies. The signal to be controlled is fed to each filter in parallel and detected in both outputs. By reversing the polarity of one of the detectors and combining the dc outputs, the voltage produces a discriminator characteristic as the controlled frequency is swept through the ferrimagnetic resonance frequencies of the two filters. By using this dc voltage in a feedback control system, the BWO frequency can be stabilized at the center of the discriminator characteristic. To sweep the BWO over a range of frequencies in either type, the dc magnetic bias that determines the ferrimagnetic resonance frequencies of the resonators can be electronically varied.

A number of practical problems exist with each type. The wobbulation system for the Pound discriminator requires additional circuitry. The filters and detectors of the two-resonator electronically-tuned discriminator must be physically matched in order to track a large frequency range and a number of transmission line coupling elements are still required. The results reported in this investigation indicate that the "discriminator" characteristic of a single resonator located in an iris may perform the same function and simplify the construction and control problems. Wobbulation circuitry and tracking would no longer be necessary. Since only one resonator is required, the discriminator would be reduced in size to essentially one-half the volume of the two-resonator system.

Another application related to the one just described is the utilization of the structure as a true frequency discriminator for the detection of frequency modulated microwave signals. In the application above, the linearity of the output was not extremely important. For detection of

frequency modulated signals, phase and amplitude linearity are important. Therefore, the response characteristics of the structure described herein must be investigated in greater detail at low values of initial attenuation to determine whether or not the output was sufficiently linear for undistorted detection of data and/or voice signals.

Other applications related to electronically-tuned band pass and band reject filters are definitely possible. There are undoubtedly a large number of other possibilities unknown at the present time which may appear during future investigations. Areas of research which warrant consideration for future investigation include: (1) A more rigorous analysis of the approximations applied to the electromagnetic field problem which were introduced by the resonator being placed at the center of the aperture, (2) development of transmission and reflection coefficient equations for analogous stripline and waveguide structures, (3) an examination of the effects of aperture shape on the experimental attenuation characteristics, (4) investigation of multiple-resonator filters, and (5) investigation of multiple-resonator, multiple-iris filters.

VI. BIBLIOGRAPHY

1. Fay, C. E. Ferrite tuned resonant cavities. IRE Proceedings 44: 1446-1449. 1956.

2. Nelson, C. E. Ferrite-tunable microwave cavities and the introduction of a new reflectionless, tunable microwave filter. IRE Proceedings 44: 1449-1455. 1956.

3. Burgess, J. H. Ferrite tunable filter for use in S-band. IRE Proceedings 44: 1460-1461. 1956.

4. DeGrasse, R. W. Low loss gyromagnetic coupling through single crystal garnets. J. Appl. Phys. 30: 155S-156S. 1959.

5. Carter, P. S., Jr. Magnetically-tunable microwave filters employing single crystal garnet resonators. IRE International Conv. Record Part 3: 130-135. 1960.

6. _____. Magnetically-tunable microwave filters using single-crystal yttrium-iron-garnet resonators. IRE Trans. on Microwave Theory and Techniques MTT-9: 252-260. 1961.

7. Patel, C. N. Magnetically tunable non-reciprocal band-pass filters using ferrimagnetic resonators. IRE Trans. on Microwave Theory and Techniques MTT-10: 152-161. 1964.

8. Kotzebue, K. L. Broadband electronically-tuned microwave filters. IRE WESCON Conv. Record Part 1: 21-27. 1960.

9. Blau, R. YIG microwave electronically tunable preselectors. Microwave Journal 6: 72-74. 1963.

10. Wright, M. L. and J. J. Taub. Miniature electrically tunable YIG band-pass filter. IRE Proceedings 50: 2107. 1962.

11. Harrison, G. R. and L. R. Hodges, Jr. Microwave properties of polycrystalline hybrid garnets. Microwave Journal 4: 53-59. 1961.

12. Severin, H. Ferrites, materials and applications. Electro Technology 71: 146-151. 1963.

13. Nielson, J. W., D. A. Lepore, J. Zneimer and G. B. Townsend. Effect of mechanical, thermal and chemical treatment of the ferrimagnetic resonance linewidth on lithium ferrite crystals. J. Appl. Phys. 33: 1379S-1380S. 1962.

14. Harvey, R. L., I. Gordon and R. A. Braden. The effect of a d-c magnetic field on the uhf permeability and losses of some hexagonal

magnetic compounds. Radio Corp. of America Rev. 22: 648-657. 1961.

15. Matthaei, G. L., L. Young and E. M. T. Jones. Design of microwave filters, impedance-matching networks, and coupling structures, Vol. 2. Menlo Park, Calif., Stanford Research Institute. (Prepared for U. S. Army Electronics Research and Development Laboratories, Fort Monmouth, New Jersey. Contract DA 36-039 SC-87398.) 1963.

16. Lax, B. and K. J. Button. Microwave ferrites and ferrimagnetics. New York, N. Y., McGraw-Hill Book Co., Inc. c1962.

17. Dekker, A. J. Solid state physics. Fifth printing. Englewood Cliffs, N. J., Prentice-Hall, Inc. 1961.

18. Osborn, J. A. Demagnetizing factors of the general ellipsoid. Phys. Rev. 67: 351-357. 1945.

19. Kittel, C. On the theory of ferromagnetic resonance absorption. Phys. Rev. 73: 155-161. 1948.

20. Hawiczka, B. and A. R. Mortis. Gyromagnetic resonance graphical design data. IEE Proceedings 110: 665-670. 1963.

21. Cunningham, J. R., Jr. and E. E. Anderson. Samarium substitutions in yttrium iron garnet. J. Appl. Phys. 31: 45S-46S. 1960.

22. McDuffie, G. E., Jr., J. R. Cunningham, Jr. and E. E. Anderson. Initial permeability characteristics of mixed yttrium-gadolinium iron garnets. J. Appl. Phys. 31: 47S-48S. 1960.

23. Dillon, J. F., Jr. and J. W. Nielson. Ferrimagnetic resonance in impurity doped yttrium iron garnet (YIG). J. Appl. Phys. 31: 43S-44S. 1960.

24. _____ and _____. Ferrimagnetic resonance in rare-earth doped yttrium iron garnet. Phys. Rev. 120: 105-113. 1960.

25. Rodrigue, G. P., J. E. Pippin, W. P. Wolf and C. L. Hogan. Ferrimagnetic resonance in some polycrystalline rare earth garnets. IRE Trans. on Microwave Theory and Techniques MTT-6: 83-91. 1958.

26. Spencer, E. G., R. C. LeCraw and C. S. Porter. Ferromagnetic resonance line width in yttrium iron garnet single crystal. Physical Review 110: 1311-1313. 1958.

27. Spencer, E. G. and R. C. LeCraw. Line width narrowing in gallium substituted yttrium iron garnet. (Abstract) Bulletin of Am. Phys. Society 5: 58. 1960.

28. White, R. L. Observations on line width in ferrimagnetic resonance. J. Appl. Phys. 30: 182S-183S. 1959.

29. Carter, P. S., Jr. and C. Flammer. Unloaded Q of single crystal yttrium-iron-garnet resonators as a function of frequency. IRE Trans. on Microwave Theory and Techniques MTT-8: 570-571. 1960.

30. Douthett, D. and I. Kaufman. The unloaded Q of a YIG resonator from X-band to 4 millimeters. IRE Trans. on Microwave Theory and Techniques MTT-9: 261-262. 1961.

31. Walker, L. R. Magnetostatic modes in ferromagnetic resonance. Phys. Rev. 105: 390-399. 1957.

32. Fletcher, P. C. and R. O. Bell. Ferrimagnetic resonance modes in spheres. J. Appl. Phys. 30: 687-698. 1959.

33. Fletcher, P. C., I. H. Solt, Jr. and R. O. Bell. Identification of the magnetostatic modes of ferrimagnetic resonance spheres. Phys. Rev. 114: 739-745. 1959.

34. Van Bladel, J. Electromagnetic fields. New York, N. Y., McGraw-Hill Book Co., Inc. 1964.

35. Marcuvitz, N., ed. Waveguide handbook. New York, N. Y., McGraw-Hill Book Co., Inc. 1951.

36. Bloembergen, N. B. and R. V. Pound. Radiation damping in magnetic resonance experiments. Phys. Rev. 95: 8-12. 1954.

37. Maslennikova, V. V. Ferrite sphere in a coaxial waveguide. (Translation) Radio Engineering and Electronic Physics 9: 499-506. 1964.

38. Gurevich, A. G. Ferrite ellipsoid in a waveguide. (Translation) Radio Engineering and Electronics 8, No. 5: 799-808. 1963.

39. Comstock, R. L. Synthesis of filter-limiters using ferrimagnetic resonators. IEEE Trans. on Microwave Theory and Techniques MTT-10: 599-607. 1964.

VII. ACKNOWLEDGMENTS

The preparation of this dissertation represents the attainment of a long sought goal. The writer has succeeded primarily as a result of the support, patience and understanding of his wife and family. But he also owes a large debt of gratitude to the many persons who have given assistance and encouragement over a period of many years. Special thanks go to the teachers and instructors who have provided the necessary academic guidance, and in particular to Drs. A. A. Read and W. B. Boast for their interest and encouragement. He wishes to acknowledge the assistance received from the Collins Radio Company wherein he was supplied with experimental devices, special facilities and a leave-of-absence authorization. He also wishes to thank Dr. W. J. Jameson for able assistance in the form of programs for the IBM 7074 computer. The help of Mmes. Mary Lou Harrison and Bonna Basler in the final preparation of this dissertation is most gratefully acknowledged.